NAME	PATRICK WALSH
I.D.	16177789
SUPERVISOR	IAN CLANCY
COURSE	B.Sc. APPLIED PHYSICS
YEAR	FOURTH YEAR
PROJECT TITLE	THE DYNAMICS OF FREELY SPINNING OBJECTS ON FRICTIONAL SURFACES
DATE	24th April 2020

Contents

When a disk is spun on a frictional surface, the trajectory of the disk is extremely sensitive to initial conditions and, under the right circumstances, can display chaotic behaviour. This paper details the use of MATLAB to develop a model which can simulate the motion of such a spinning disk system, explores the most influential initial conditions of the disk in terms of changing the behaviour of the disk in motion, studies the exact relationship between each of these initial conditions and the trajectory of the centre of mass and ultimately analyses the effect of possibly the most affective initial condition on the amount of chaos exhibited by the spinning disk system using the theory of Lyapunov exponents. The results detailed show a relation between the level of chaos exhibited by the system and the level of retrograde experienced by the centre of mass motion with the sensitivity increasing dramatically as the initial condition approaches its maximum value.

1. Introduction

1.1. The dynamics of spinning objects

When modelling a spinning disk, the concept of Euler's disk is used define the disks motion and its degrees of freedom. The motion of a spinning/rolling disk can be modelled in terms of Euler vectors and Euler angles. Consider a disk as illustrated in Figure 1.1: Graphic of the relevant vectors and angles of Euler's disk. [1] (Detailed also in Literature review)

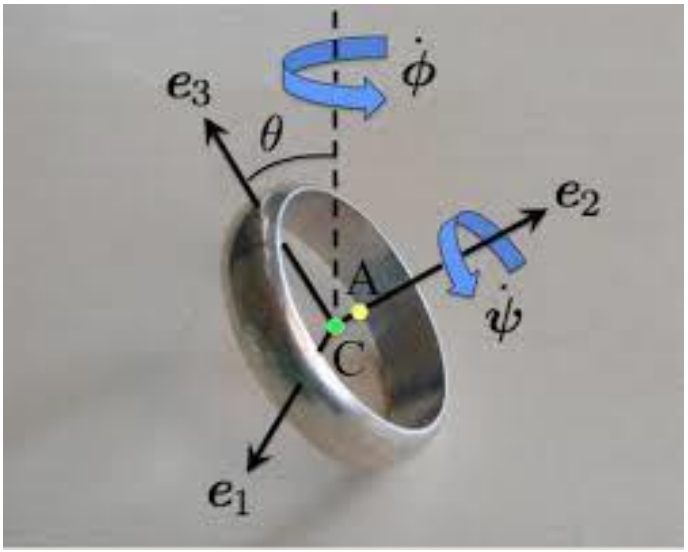

Figure 1.1: Graphic of the relevant vectors and angles of Euler's disk

The diagram above helps to visualise the physical meaning of all of the Euler vectors and angles. The vectors e_1, e_2 and e_3 represent the Euler vectors in the frame of the disk. e_1 always points parallel to the surface, e_3 is perpendicular to e_1 in the plane of the disk (pointing away from the point of contact with the surface) and e_2 points through the axis of symmetry of the disk, perpendicular to both e_1 and e_3.

The Euler angles θ, ψ and ϕ represent the nutation (tilt), the revolution (about e_2) and the precession of the disk about the vertical.

Outside of the rotating frame of the disk, an inertial frame is defined which helps to model the motion of the centre of mass of the disk and the contact point A between the disk and the flat surface. The basis for this frame is taken as $(\hat{\imath}, \hat{\jmath}, \hat{k})$ and the co-ordinates used to describe the position of a point on the disk in the inertial frame are (x, y, z).

Using this model, the disk has six degrees of freedom; $(x, y, z, \theta, \phi, \psi)$. These quantities are related to one another through second order ordinary differential equations. The

notation involved in these ODEs tends to change based on which piece of literature one is looking at. Some relevant symbols are defined as follows for the entirety of this study:

- $a \equiv disk\ radius$
- $h \equiv disk\ width$
- $m \equiv disk\ mass$
- $g \equiv gravitational\ acceleration$
- $C_i \equiv drag\ coefficients$

1.2.The Equations of Motion

Many of these ODEs can be easily expressed in matrix form and are all inter-related. The ultimate goal is to solve for the six degrees of freedom $(x,\ y,\ z,\ \theta,\ \phi,\ \psi)$. To achieve this, we develop three sets of ODEs in terms of nine main quantities:

1. The three components of the disk's angular velocity $(\omega_1,\ \omega_2,\ \omega_3)$
2. The three Euler angles $(\theta,\ \phi,\ \psi)$
3. The three position co-ordinates of the disk's centre of mass $(x,\ y,\ z)$

1. The three components of the disk's angular velocity. The angular velocity vector $\vec{\boldsymbol{\omega}}$ can be found by solving the ODE in Equation 1.1 below. The necessary components of this equation are defined also:

$$\underline{\boldsymbol{J}}.\dot{\vec{\boldsymbol{\omega}}} = -\vec{\boldsymbol{\Omega}} \times \overrightarrow{\boldsymbol{L_G}} - m\,\overrightarrow{\boldsymbol{r_G}} \times \left(\vec{\boldsymbol{\Omega}} \times \overrightarrow{\boldsymbol{v_c}}\right) + mg\left[a\sin(\theta) - \frac{h}{2}\cos(\theta)\right]\widehat{\boldsymbol{e_1}} + \vec{\boldsymbol{T}}_{\boldsymbol{Drag}}$$

Equation 1.1: First order differential equation of the disk angular velocity

$$\underline{\boldsymbol{I}} = m\begin{bmatrix} \frac{3a^2+h^2}{12} & 0 & 0 \\ 0 & \frac{a^2}{2} & 0 \\ 0 & 0 & \frac{3a^2+h^2}{12} \end{bmatrix}, \qquad \underline{\boldsymbol{J}} = \underline{\boldsymbol{I}} + m\begin{bmatrix} \frac{h^2}{4}+a^2 & 0 & 0 \\ 0 & a^2 & -\frac{ah}{2} \\ 0 & -\frac{ah}{2} & \frac{h^2}{4} \end{bmatrix}$$

Equation 1.2: Inertia tensor of disk

$$\vec{\boldsymbol{\omega}} = \begin{bmatrix} \dot{\theta} \\ \dot{\phi}\sin(\theta) + \dot{\psi} \\ \dot{\phi}\cos(\theta) \end{bmatrix}$$

Equation 1.3: Angular velocity of disk

$$\vec{\boldsymbol{\Omega}} = \vec{\boldsymbol{\omega}} - \dot{\psi}\boldsymbol{e_2} = \begin{bmatrix} \dot{\theta} \\ \dot{\phi}\sin(\theta) \\ \dot{\phi}\cos(\theta) \end{bmatrix}$$

Equation 1.4: Angular velocity of moving frame

$$\overrightarrow{\boldsymbol{L_G}} = \underline{\boldsymbol{I}}.\vec{\boldsymbol{\omega}}$$

Equation 1.5: Angular momentum of disk wrt contact point

$$\overrightarrow{\boldsymbol{r_G}} = \begin{bmatrix} 0 \\ h/2 \\ 0 \end{bmatrix}$$

Equation 1.6: Position of center of mass wrt contact point

$$\overrightarrow{\boldsymbol{v_C}} = \dot{\overrightarrow{\boldsymbol{r_C}}} = \vec{\boldsymbol{\omega}} \times \overrightarrow{\boldsymbol{r_G}}$$

Equation 1.7: Velocity of center of mass wrt fixed frame

$$\vec{\boldsymbol{T}}_{\boldsymbol{Drag}} = -\underline{\boldsymbol{J}}\sum_{i}^{3} C_i|\omega_i|\omega_i.\boldsymbol{e_i}$$

Equation 1.8: Drag induced torque of disk

Once Equation 1.2 through Equation 1.8 are defined in MATLAB, Equation 1.1 can be defined. This is a first order ODE in $\vec{\boldsymbol{\omega}}$**.** Equation 1.1 is expressed in terms of $\dot{\vec{\boldsymbol{\omega}}}$ and is

defined by its own function ‘Domega’. This equation is then manipulated to find an equation for the Euler angle derivatives:

2. The three Euler angles. One defines a matrix ‘o2DE’ to transform $\vec{\boldsymbol{\omega}}$ to $\begin{bmatrix}\dot{\theta}\\ \dot{\phi}\\ \dot{\psi}\end{bmatrix}$:

$$o2DE = \begin{bmatrix}1 & 0 & 0\\ 0 & 1 & -\tan(\theta)\\ 0 & 0 & \dfrac{1}{\cos(\theta)}\end{bmatrix}$$

Equation 1.9: Transformation matrix to produce the Euler angle ODEs from $\vec{\omega}$

$$DEuler = o2DE * omega$$

Equation 1.10: Euler angle ODE set

This provides the second set of first order ODEs

3. The three position co-ordinates of the disk’s centre of mass. The position co-ordinates can be defined in a similar way as above using the Euler angles this time.

A function ‘Euler2Cartesian’ is defined which sets the value of three transformation functions:

$$R_1(\alpha) = \begin{bmatrix}1 & 0 & 0\\ 0 & \cos(\alpha) & \sin(\alpha)\\ 0 & -\sin(\alpha) & \cos(\alpha)\end{bmatrix}$$

$$R_2(\alpha) = \begin{bmatrix}\cos(\alpha) & 0 & -\sin(\alpha)\\ 0 & 1 & 0\\ \sin(\alpha) & 0 & \cos(\alpha)\end{bmatrix}$$

$$R_3(\alpha) = \begin{bmatrix}\cos(\alpha) & \sin(\alpha) & 0\\ -\sin(\alpha) & \cos(\alpha) & 0\\ 0 & 0 & 1\end{bmatrix}$$

Equation 1.11: Transformation functions to convert from angular to cartesian form

Two functions are then defined; C2E and E2C to convert from cartesian to angular form and back. This makes it easier to convert from Euler to cartesian as one can solve the easier form of cartesian to angular and then invert the matrix to convert the other way:

$$C2E = R_1(\theta) * R_3(\phi), \qquad E2C = inv(C2E)$$

R_2 is not needed here as only θ and ϕ are needed to determine the cartesian position given a fixed radius, a. The centre of mass does not move as the revolution angle ψ changes.

The position ODE set is then expressed as:

$$Dposition = E2C(Euler) * \overrightarrow{\boldsymbol{v_c}}$$

Equation 1.12: Position co-ordinates ODE set.

This gives us three functions; Dposition, DEuler and Domega, each representing three ODEs. These functions can then be concatenated into one function of nine ODEs to be solved in parallel:

1.3. Solving the ODEs

Solving these ODEs in MATLAB, one requires the use of an ODE solver. The one that will be used throughout this project is ODE45. The numerical method this is working behind the scenes when ODE45 is called. The method takes in the concatenated function $[Dposition; DEuler; Domega]$ ($func$ below) and solves the ODEs involved numerically. The Integration times and the initial values of the position, Euler angles and omega vector are also set.

```
[t, x] = ode45(@(t, x)ConcatenatedFunction, IntegrationTimes, [position;
 Euler0; omega0], opts);
```

The numerical method that the ODE45 method is based on is detailed below

1.4. The ODE45 method

The working principal of ODE45 is based on the Runge-Kutta method. A Runge-Kutta method is a numerical analysis technique used to approximately solve an ordinary differential equation. They are used heavily in computation when finding analytical solutions can be challenging. These methods can be implicit or explicit methods; the RK4 method (which is generally referred to as 'the runge-kutta method') is an example of an explicit numerical method. There are infinitely many iterations of the Runge-Kutta method (1^{st} order, 2^{nd} order, …, n^{th} order) each one more accurate than the last. Each time the order is increased, the accuracy increases by a smaller and smaller amount i.e. most of the accuracy of the method is achieved in the first few orders; similar to a Taylor series expansion. The ODE45 method is so named as it employs 4^{th} and 5^{th} order RK methods to solve the ODE. A 5^{th} order RK method is used to solve the ODEs, then the process is repeated, this time using a 4^{th} order RK method. The two results are then compared and if they are not sufficiently close, the time step used for the RK methods is narrowed and the process repeated. This process is repeated until the results of the 4^{th} and 5^{th} order RK methods are within a certain degree of closeness, at which point the solution is accepted as sufficiently accurate.

The general formulae for solving an explicit RK method is based on discrete iterations, and so a step size must be set. The iterative value of the function y is given by

$$y_{n+1} = y_n + h\sum_{i=1}^{s} b_i k_i$$

Equation 1.13: Iterative formula for solving y from ẏ

where

$$\dot{y} = f(t, y), \qquad y(t_0) = y_0$$

The time step is then set to be h such that

$$t_{n+1} = t_n + h$$

The values of k_i in Equation 1.13 are given by the general form [4]

$$k_1 = f(t_n, y_n)$$

$$k_2 = f\big(t_n + c_2 h, y_n + h(a_{21} k_1)\big)$$

$$k_3 = f\big(t_n + c_3 h, y_n + h(a_{31} k_1 + a_{32} k_2)\big)$$

$$\vdots$$

$$k_s = f\left(t_n + c_s h, y_n + h\big(a_{s1} k_1 + a_{s2} k_2 + \cdots + a_{s,s-1} k_{s-1}\big)\right)$$

Only first order equations can be solved by a RK4 or RK5 method, therefore if trying to solve a second order equation using ODE45, such an ODE would need to be expressed as two first order ODEs as in the following example:

$$\ddot{x} = \dot{x} + x$$

becomes

$$\dot{x}(1) = x(2)$$

$$\dot{x}(2) = x(2) + x(1)$$

Here $x(1)$ represents x and $x(2)$ represents $\dot{x}$.

This numerical method is encoded into ODE45 and solves the equations of motion of the spinning disk system creating a working model on which to run simulations. The model can therefore be used to answer some interesting questions such as how sensitive the disk is to each initial condition on which it depends.

1.5. Variation of initial conditions

There are a number of parameters of the system which should influence the behaviour of the disk's motion. These include;

- The disk's radius, a
- The disk's mass, m
- The disk's thickness, h
- Acceleration due to gravity, g
- The initial nutation and initial rate of nutation, θ and $\dot{\theta}$
- The initial rate of precession, $\dot{\phi}$

The effect of these parameters on the motion of the disk can be analysed by running the model for two separate sets of initial conditions and watching the change in behaviour of the system. This can shed light on how chaotic the system is. However, this analysis is very qualitative and is worth far more if there is a quantitative way of analysing the degree of sensitivity of the system to each initial condition. This is where Lyapunov exponents come in and give an easily expressible numerical value to the level of chaos that the system exhibits.

1.6.Lyapunov exponents

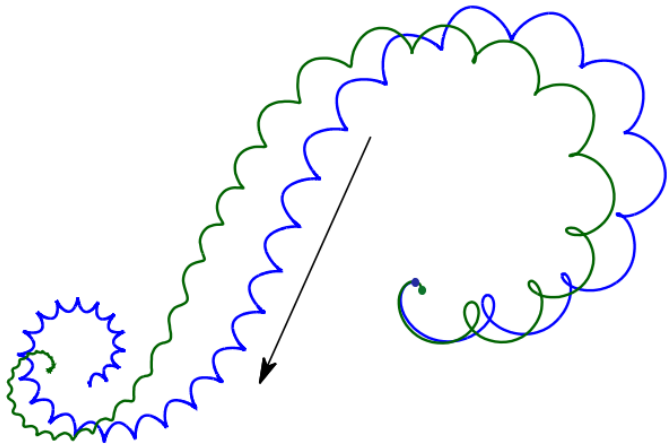

Figure 1.2: Difference in path of a chaotic system using different initial conditions (exaggerated).

The concept of Lyapunov exponents are used to describe the level of chaos exhibited by a system. The basic idea involves defining two varying initial positions for the system to run from. (These initial positions may be varied directly or indirectly by varying another parameter which influences the position). The initial positions can be defined as x_0 and $x_0 + \epsilon$ and the difference d_n after n iterations (can also be expressed as time, t) will diverge exponentially in a chaotic system according to the equation:

$$d_t = \epsilon e^{\lambda t}$$

Equation 1.14: Lyapunov's formula

The λ in Equation 1.14 is referred to as the Lyapunov exponent. If λ is negative, the equation above implies that the difference will approach 0 and the points will converge (meaning the system is not chaotic). If, however it is positive then they will diverge. The magnitude of the positive Lyapunov exponent indicates how chaotic the system is; in other words, how much the paths will diverge in a given time interval from a tiny change in the initial conditions of the system.

The value of λ can be easily determined by taking the log of both sides of Equation 1.14:

$$\ln(d_n) = \ln(\epsilon) + \lambda t$$

Equation 1.15: Natural log of Lyapunov's formula

A graph can easily be generated of $\ln(d_n)$ vs t and the initial slope of this graph can be taken as the Lyapunov exponent.

1.7. The edge of chaos

This study of the effect of the initial conditions of the system on its tendency to behave chaotically can lead into a further analysis of how exactly the initial conditions need to be changed to incite chaos. From here, one can figure out the exact initial conditions at which chaos sets in, the point that is sometimes referred to as 'the onset of chaos' or 'the edge of chaos'. This is beyond the scope of this project, however, this project along with the model used could serve as a foundation for this type of study.

1.8. Project aims

The aims of this project are to model the trajectory of the centre of mass of the spinning disk by looking at the physical path it takes, the variation in the disk's angular velocity and the evolution of the angle of nutation over time, to study how this behaviour depends on the initial conditions and to analyse the Lyapunov exponent of the system and finally, to study the effect of friction on the trajectory of the disk.

2. Literature Review

2.1. The inertia tensor

The concept of the inertia tensor is useful in modelling the centre of mass of the spinning object as it moves in three dimensions. To build up the concept of the Inertia tensor we first look at some useful formulas. [5]

The rotational inertia of a system is given by

$$I = MR^2$$

Consider a rigid body which is rotating with an angular velocity ω while also moving with a linear velocity V. The instantaneous velocity of a point α on the body can be expressed as

$$v_\alpha = V + \omega \times r_\alpha$$

$$T = \frac{1}{2}\sum_\alpha m_\alpha (V + \omega \times r_\alpha)^2$$

$$T = T_T + T_R$$

$$T_T = Translational\ Kinetic\ Energy, \qquad T_R = Rotational\ Kinetic\ Energy$$

$$T_T = \frac{1}{2}\sum_\alpha m_\alpha V^2\,, \qquad T_R = \frac{1}{2}\sum_\alpha m_\alpha (\omega \times r_\alpha)^2$$

But, the square of a cross product can be expanded as

$$(A \times B)^2 = A^2B^2 - (A \cdot B)^2$$

$$T_R = \frac{1}{2}\sum_\alpha m_\alpha (\omega^2 r_\alpha^2 - (\omega \cdot r_\alpha)^2)$$

Let the position r_α be represented by the co-ordinates

$$r_\alpha = \left(x_{\alpha,1}, x_{\alpha,2}, x_{\alpha,3}\right)$$

This results in the relationship for the rotational kinetic energy

$$T_R = \frac{1}{2}\sum_{ij} \omega_i \omega_j \sum_\alpha m_\alpha \left(\delta_{ij} \sum_k x_{\alpha,k}^2 - x_{\alpha,i} x_{\alpha,j}\right)$$

This allows us to define an Inertia term in i and j

$$T_R = \frac{1}{2}\sum_{ij} I_{ij} \omega_i \omega_j\,, \qquad I_{ij} = \sum_\alpha m_\alpha \left(\delta_{ij} \sum_k x_{\alpha,k}^2 - x_{\alpha,i} x_{\alpha,j}\right)$$

The TR term above takes the expected form

$$T_R = \frac{1}{2} I \omega^2$$

The 9 values of I_{ij} constitute I which is referred to as the inertia tensor. The tensor is needlessly cumbersome and less readable in its state defined by letting $r_\alpha = \left(x_{\alpha,1}, x_{\alpha,2}, x_{\alpha,3}\right)$ so this term is redefined as

$$r_\alpha = (x_\alpha, y_\alpha, z_\alpha)$$

This allows the inertia tensor to be written as

$$\{I\} = \begin{bmatrix} \sum_\alpha m_\alpha (r_\alpha^2 - x_\alpha^2) & -\sum_\alpha m_\alpha x_\alpha y_\alpha & -\sum_\alpha m_\alpha x_\alpha z_\alpha \\ -\sum_\alpha m_\alpha y_\alpha x_\alpha & \sum_\alpha m_\alpha (r_\alpha^2 - y_\alpha^2) & -\sum_\alpha m_\alpha\, y_\alpha z_\alpha \\ -\sum_\alpha m_\alpha z_\alpha x_\alpha & -\sum_\alpha m_\alpha z_\alpha y_\alpha & \sum_\alpha m_\alpha (r_\alpha^2 - z_\alpha^2) \end{bmatrix}$$

The I_{ij} term can be re-written for a body with a continuous matter distribution and mass density ρ [5]

$$\rho = \rho(r)$$

$$I_{ij} = \int_V \rho(r)\left(\delta_{ij}\sum_k x_k^2 - x_i x_j\right)dV, \qquad dV = dx_1 dx_2 dx_3$$

2.2.Euler vectors/Euler angles

2.2.1. Terminal retrograde turn of rolling rings

This paper by Jalali et al. [1] provided the framework for the model used in this project. The notation is detailed in the introduction and Figure 1.1 and the equations are reiterated:

$$\underline{\boldsymbol{I}}.\dot{\vec{\boldsymbol{\omega}}} - m\overrightarrow{\boldsymbol{r_G}} \times \left(\overrightarrow{\boldsymbol{r_G}} \times \dot{\vec{\boldsymbol{\omega}}}\right) = -\vec{\boldsymbol{\Omega}} \times \overrightarrow{\boldsymbol{L_G}} - m\,\overrightarrow{\boldsymbol{r_G}} \times \left(\vec{\boldsymbol{\Omega}} \times \overrightarrow{\boldsymbol{v_c}}\right) + mg\left[a\sin(\theta) - \frac{h}{2}\cos(\theta)\right]\widehat{\boldsymbol{e_1}}$$

Equation 2.1: Angular velocity ODE in terms of Inertia

$$\underline{\boldsymbol{J}}.\dot{\vec{\boldsymbol{\omega}}} = -\vec{\boldsymbol{\Omega}} \times \overrightarrow{\boldsymbol{L_G}} - m\,\overrightarrow{\boldsymbol{r_G}} \times \left(\vec{\boldsymbol{\Omega}} \times \overrightarrow{\boldsymbol{v_c}}\right) + mg\left[a\sin(\theta) - \frac{h}{2}\cos(\theta)\right]\widehat{\boldsymbol{e_1}} + \vec{\boldsymbol{T}}_{\boldsymbol{Drag}}$$

(Equation 1.1)

$$\underline{\boldsymbol{J}} = \underline{\boldsymbol{I}} + m\begin{bmatrix} \frac{h^2}{4} + a^2 & 0 & 0 \\ 0 & a^2 & -\frac{ah}{2} \\ 0 & -\frac{ah}{2} & \frac{h^2}{4} \end{bmatrix}$$

(Equation 1.2)

$$\vec{\boldsymbol{T}}_{\boldsymbol{Drag}} = -\underline{\boldsymbol{J}}\sum_i^3 C_i|\omega_i|\omega_i.\boldsymbol{e_i}$$

(Equation 1.8)

The value of *I* used by Jalali and in Equation 1.2 can be found in the literature [2]:

$$\underline{\boldsymbol{I}} = m\begin{bmatrix} \frac{3a^2+h^2}{12} & 0 & 0 \\ 0 & \frac{a^2}{2} & 0 \\ 0 & 0 & \frac{3a^2+h^2}{12} \end{bmatrix}$$

(Equation 1.2)

2.2.2. Rolling Friction and Energy Dissipation in a spinning disk

Daolin Ma and their team [3] use the illustration in Figure 2 to visualise the disk:

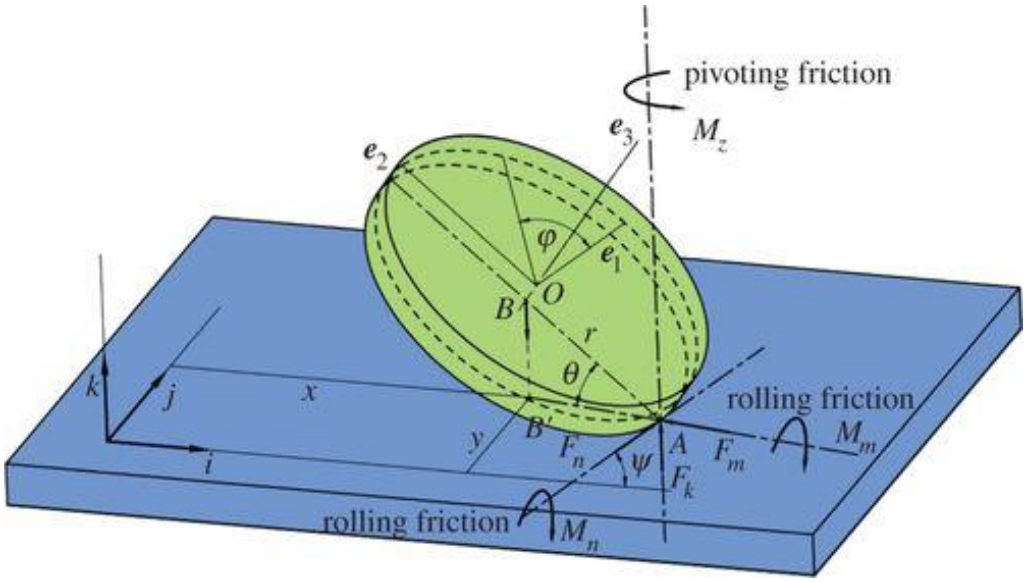

Figure 2.1: Euler's disk illustration (Ma et al.)

Note the notation difference as opposed to the paper by Jalali et al. where $\boldsymbol{e_2}$ and $\boldsymbol{e_3}$ are reversed as are ϕ and ψ. As stated earlier, the disk has six degrees of freedom; $(x, y, z, \psi, \theta, \phi)$ which are related to one another through second order ODEs.

The radius is defined in this paper as r. The inertia tensor of the disk is defined as J with principal moments J_1, J_2 and J_3.

$$J_1 = J_2 = \frac{1}{4}mr^2 + \frac{1}{3}mh^2, \qquad J_3 = \frac{1}{2}mr^2$$

The absolute angular velocity of a point on the disk is Ω.

$$\vec{\boldsymbol{\Omega}} = \begin{bmatrix} \omega_1 \\ \omega_2 \\ \omega_3 \end{bmatrix}$$

Keeping this in mind, the angular momentum $\overrightarrow{\boldsymbol{L_O}}$ about the centre of mass is written as

$$\overrightarrow{\boldsymbol{L_O}} = \begin{bmatrix} J_1\omega_1 \\ J_1\omega_2 \\ J_3\omega_3 \end{bmatrix}$$

We can define another co-ordinate frame at the point of contact A between the disk and the surface.

$$R_A = \begin{bmatrix} \boldsymbol{m^0} \\ \boldsymbol{n^0} \\ \boldsymbol{k} \end{bmatrix}$$

Defining this allows us to introduce the resultant force $\overrightarrow{\boldsymbol{F_A}}$ and the net moment $\overrightarrow{\boldsymbol{M_A}}$ of the surface acting on the disk at the contact point A.

$$\overrightarrow{\boldsymbol{F_A}} = \begin{bmatrix} F_n \\ F_m \\ F_z \end{bmatrix}, \qquad \overrightarrow{\boldsymbol{M_A}} = \begin{bmatrix} M_n \\ M_m \\ M_z \end{bmatrix}$$

With this in mind the equations for the centre of mass are:

$$\begin{bmatrix} \dot{x} \\ \dot{y} \\ \dot{z} \end{bmatrix} = \begin{bmatrix} \cos(\psi) & \sin(\psi) & 0 \\ -\sin(\psi) & \cos(\psi) & 0 \\ 0 & 0 & 1 \end{bmatrix} + \begin{bmatrix} \dot{\psi}\big(rcos(\theta) - hsin(\theta)\big) + \dot{\phi}r \\ \dot{\theta}\big(rsin(\theta) + hcos(\theta)\big) \\ \dot{\theta}\sin(\theta)\,(h - r) \end{bmatrix}$$

Equation 2.2: Centre of mass position ODEs. [3]

And the angular equations:

$$I_1\ddot{\theta} - I_2\dot{\psi}^2\sin(\theta)\cos(\theta) + \big(I_3\sin(\theta) + mrhcos(\theta)\big)\dot{\psi}\omega_3 - mrh\dot{\psi}^2\sin^2(\theta) + mg\big(rcos(\theta) - hsin(\theta)\big) = 0$$

$$I_2\frac{d}{dt}\big(\dot{\psi}\sin(\theta)\big) + J_1\dot{\theta}\dot{\psi}\cos(\theta) - J_3\dot{\theta}\omega_3 - mhr\dot{\omega}_3 + mh\dot{\psi}\dot{\theta}\big(rsin(\theta) + hcos(\theta)\big) = 0$$

$$I_3\dot{\omega}_3 - mrh\frac{d}{dt}\left(\dot{\psi}\sin(\theta)\right) - mr\dot{\psi}\dot{\theta}\left(rsin(\theta) + hcos(\theta)\right) = 0$$

Equation 2.3: Euler angle ODEs. [3]

The quantities I_1, I_2 and I_3 are based on the principle moments of inertia J:

$$\begin{bmatrix} I_1 \\ I_2 \\ I_3 \end{bmatrix} = \begin{bmatrix} J_1 + m(h^2 + r^2) \\ J_1 + mh^2 \\ J_3 + mr^2 \end{bmatrix}$$

The energy of the system remains constant during the rolling motion due to a lack of dissipation:

$$E = \frac{1}{2}m(\dot{x}^2 + \dot{y}^2 + \dot{z}^2) + \frac{1}{2}(J_1\omega_1^2 + J_1\omega_2^2 + J_3\omega_3^2) + mgz$$

Equation 2.4: Constant energy term. [3]

The results of this study were not obtained by simulation, but rather by spinning a disk and recording the motion of the centre of mass with a high-speed camera. This means that the equations of motion in this study have not been used to generate the results in Figure 2.2: Nutation θ vs timeFigure 2.2 and Figure 2.3

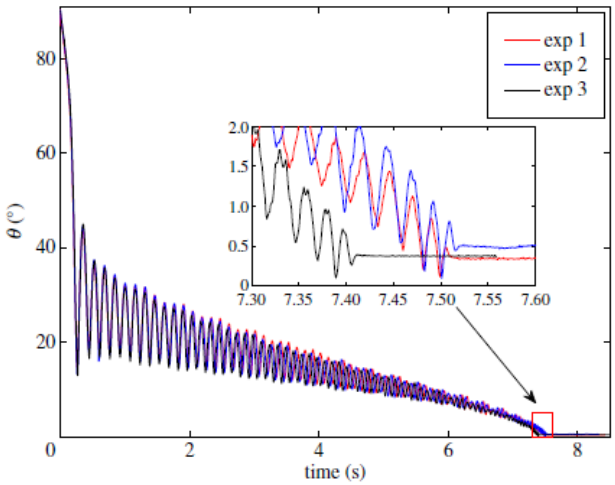

Figure 2.2: Nutation θ vs time. [3]

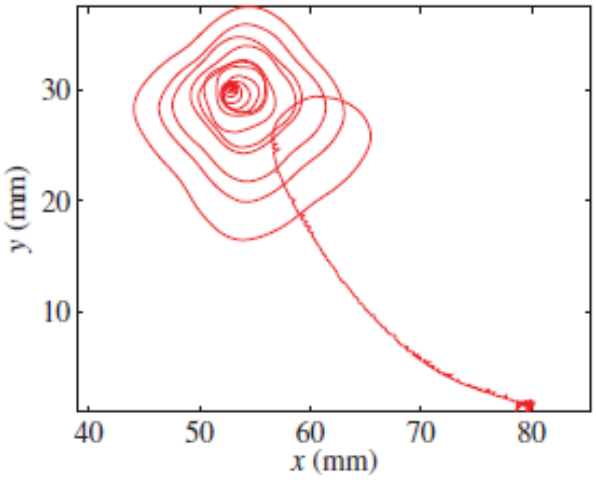

Figure 2.3: Path of centre of mass in x-y plane. [3]

This is the paper on which this project's model was originally based however, due to the complexity of the equations involved and the abundance of approximations and assumptions in the study, this model is impractical for simulating the results that Daolin Ma and his team obtained. The results obtained by Ma were not directly based on the equations of motion specified; these equations were derived separately as background theory. This model was abandoned and Jalali's equations of motion were used instead as the equations involved were more fundamental and, from a modelling perspective, more practical.

3. Simulated Model

All of the code used throughout the project is detailed below. It may also be found on GitHub. [6] The GitHub versions may include extra comments and clarification but are functionally the same.

The following code in Figure 3.1 models the motion of the spinning disk based on the equations of motion in the introduction.

```
function [DEuler]=EqOfMotionModel()
        clear all
        m=1;  %Disk mass (g)
        g=9.8;       %Gravitation constant (m/s/s)
        a=1.0;  %Disk radius (m)
        h=2;    %Disk height (mm)
        C=[0.03, 0.073,0.185]';
        [I,J,rG]=CreateConstantMatrices(m,g,h,a);
        IntegrationTimes=0:0.0001:10;

        Euler0=deg2rad([50;0;0]);
        Euler1=deg2rad([49.999;0;0]);
        DEuler0=[0;0;80];
        DEuler1=[0;0;80];
        DE2o=@(theta)[1,0,0;0,1,sin(theta);0,0,cos(theta)];
        omega0=DE2o(Euler0(1))*DEuler0;
        omega1=DE2o(Euler1(1))*DEuler1;
        position0=[0;0;a*sin(Euler0(1))+(h/2)*cos(Euler0(1))];
        position1=[cos(Euler1(3))*(a*cos(Euler1(1))-a*cos(Euler0(1)));...
            sin(Euler1(3))*(a*cos(Euler1(1))-a*cos(Euler0(1)));...
            a*sin(Euler1(1))+(h/2)*cos(Euler1(1))];

        %ODE45 Method
        opts=odeset('RelTol',1e-4,'AbsTol',1e-5,'MaxStep',1e-1,...
            'InitialStep',1e-10,'Events',@(t,x)FallingEventFcn(t,x,a,h));
        [t,x]=ode45(@(t,x)func(t,x,I,J,rG,g,m,h,C),IntegrationTimes,...
            [position0;Euler0;omega0],opts);
        [t2,x2]=ode45(@(t,x)func(t,x,I,J,rG,g,m,h,C),IntegrationTimes,...
            [position1;Euler1;omega1],opts);

        %Position of Centre Of Mass
        figure(1)
        plot3(x(:,1),x(:,2),x(:,3))
        xlabel('x');
        ylabel('y');
        zlabel('z');
        savefig(figure(1),'CentreOfMassMotion(50v0.001,0,0,0,0,80).fig')

        %Omega vector
        figure(2)
        plot3(x(:,7),x(:,8),x(:,9))
        xlabel('\omega_1');
        ylabel('\omega_2');
        zlabel('\omega_3');
        savefig(figure(2),'AngularMomentumVector(50v0.001,0,0,0,0,80).fig')

        %Theta vs Time
        figure(3)
        plot(t,x(:,4)./pi)
        xlabel('Time, t');
        ylabel('\theta/\pi');
        savefig(figure(3),'Theta(50v0.001,0,0,0,0,80).fig')

        %Lyapunov exponent plotter
        LyapunovDiff=sqrt((x(:,1)-x2(:,1)).^2+(x(:,2)-x2(:,2)).^2+(x(:,3)-..
            x2(:,3)).^2);
```

```
57 -        figure(4)
58 -        plot(IntegrationTimes,log(LyapunovDiff))
59 -        P = polyfit(IntegrationTimes(74:187),log(LyapunovDiff(74:187)'),1);
60 -        LyapunovExponent = P(1);
61 -        LogInitialSeparation = log(LyapunovDiff(1));
62 -        YIntercept = P(2);
63 -        xlabel('Time, t');
64 -        ylabel('ln(d_t)');
65 -        savefig(figure(4),'Lyapunov(deletev0.001,0,0,0,0,80).fig')
66 -    end
67
68      function [I,J,rG]=CreateConstantMatrices(m,g,h,a)
69 -      I=diag(m.*[(3*a^2+h^2)/12,(a^2)/2,(3*a^2+h^2)/12]);
70 -      J=I+m.*[a^2+(h^2)/4,0,0;0,a^2,-a*h/2;0,-a*h/2,(h^2)/4];
71 -      rG=[0;h/2;a];
72 -    end
73
74      function [E2C]=Euler2Cartesian(Euler)
75 -      theta=Euler(1);
76 -      psi=Euler(2);
77 -      phi=Euler(3);
78 -      R1=@(angle)[1,0,0;0,cos(angle),sin(angle);0,-sin(angle),cos(angle)];
79 -      R2=@(angle)[cos(angle),0,-sin(angle);0,1,0;sin(angle),0,cos(angle)];
80 -      R3=@(angle)[cos(angle),sin(angle),0;-sin(angle),cos(angle),0;0,0,1];
81
82 -      C2E=R1(theta)*R3(phi);
83 -      E2C=inv(C2E);
84 -    end
85
86      function [Dx]=func(t,x,I,J,rG,g,m,h,C)
87 -      Euler=x(4:6);
88 -      omega=x(7:9);
89 -      theta=Euler(1);
90 -      o2DE=[1,0,0;0,1,-tan(theta);0,0,1/cos(theta)];
91 -      Omega=omega-[0;omega(2)-omega(3)*tan(theta);0];
92 -      LG=I*omega;
93 -      gvec=-g*[0;sin(theta);cos(theta)];
94 -      vc=cross(omega,rG);
95 -      taudrag=-C.*omega.*abs(omega);
96 -      Domega=J\(-cross(Omega,LG)-m*cross(rG,cross(Omega,vc))+m*...
97            cross(rG,gvec))+taudrag;
98 -      DEuler=o2DE*omega;
99 -      Dposition=Euler2Cartesian(Euler)*vc;
100 -     Dx=[Dposition;DEuler;Domega];
101 -   end
102
103     function [value,isterminal,direction] = FallingEventFcn(t,x,a,h)
104 -     isterminal=[1,1];
105 -     direction=[0,0];
106 -     value=[x(4); x(4)-pi/2];
107 -   end
```

Figure 3.1: MATLAB model of a spinning disk

Measuring the Lyapunov exponent involves taking the slope of the line of best fit of a suitable set of linear datapoints near the beginning of the plot. However, the system is

extremely sensitive to the initial conditions and so the exact location of this set of datapoints varied erratically as theta was varied. This made the range of datapoints used for the LE calculation difficult to automate. The LE was therefore calculated manually for each value of Theta. A separate script (Figure 3.2) was used to record and plot the Lyapunov exponent λ at each value of θ. These Lyapunov exponent values were then normalised against the minimum value found for $\lambda(\theta)$.

The LE values are themselves highly erratic and are very sensitive to the exact range chosen to calculate them. Care was taken to ensure that the method for selecting the range was kept as consistent as possible for all angles. For this reason, the exact values calculated for the Lyapunov exponents may not be accurate and should not be taken as exact results but rather simply as an indication of the pattern of the relative magnitude of the Lyapunov exponent with Theta. The values of the Lyapunov exponents are therefore all normalised against the minimum value.

```
%% Measuring the Lyapunov exponent involves taking the slope of the line of
%  best fit of a suitable set of linear datapoints near the beginning of
%  the plot. However, the system is extremely sensitive to the initial
%  conditions and so the exact location of this set of datapoints varied
%  erratically as theta was varied. This made the range of datapoints used
%  for the LE calculation difficult to automate. The LE was therefore
%  calculated manually for each value of Theta.
Theta = [28:89]';
LyapunovExponents = ...
    [72.6450
    70.6024
    68.5794
    72.0817
    77.2120
    85.5336
    91.7740
    98.0402
    105.2798
    107.0649
    112.8604
    122.9429
    129.5178
```

```
    136.8976
    148.8340
    152.5570
    167.0119
    173.2172
    163.9791
    153.0496
    143.2071
    136.7544
    126.0812
    122.2405
    120.3661
    113.6397
    109.9399
    107.6846
    104.8207
    97.6202
    94.6429
    93.2903
    92.2087
    89.2437
    85.3296
    81.9046
    81.5086
    78.3085
    77.7820
    77.8301
    78.7930
    79.6218
    81.5838
    83.7317
    86.7674
    88.5410
    95.8728
    99.0506
    107.5283
    109.9647
    113.7994
    127.4730
    147.8338
    164.9343
    186.3686
    205.6586
    271.4705
    275.8553
    379.4066
    631.5421
    890.1528
    2.3242e+03];

% The LE values are themselves highly erratic and are very sensitive to the
% exact range chosen to calculate them. Care was taken to ensure that the
% method for selecting the range was kept as consistent as possible for all
% angles. For this reason the exact values calculated for the Lyapunov
% exponents may not be accurate and should not be taken as exact results
% but rather simply as an indication of the pattern of the relative
```

```
79      % magnitude of the Lyapunov exponent with Theta. The values of the Lyapunov
80      % exponents are therefore all normalised against the minimum value.
81 -    NormVal = min(LyapunovExponents);
82 -    figure(1)
83 -    plot(Theta,smooth(LyapunovExponents/NormVal));
84 -    xlabel('\theta');
85 -    ylabel('\lambda');
86 -    savefig(figure(1),'Normalised Lyapunov Exponent vs Theta(Entire).fig')
```

Figure 3.2: Lyapunov exponent plotter

4. Measurements, Results and Analysis

4.1. Effect of initial θ and $\dot{\phi}$ on the behaviour along the trajectory

The trajectory of the centre of mass can be measured at any combination of initial values of θ and $\dot{\phi}$ to a significantly different result. The same reasoning applies to the change in the three components of the angular velocity, ω_1, ω_2 and ω_3 as well as the variation of the angle of nutation over time. There are too many permutations to plot so to illustrate how these parameters depend on θ and $\dot{\phi}$, we can instead generate four plots with combinations of 'high' and 'low' initial values of θ and $\dot{\phi}$.

- $\theta_{high} = 89°$
- $\theta_{low} = 45°$
- $\dot{\phi}_{high} = 80\ revolutions\ t^{-1}$
- $\dot{\phi}_{low} = 6.5\ revolutions\ t^{-1}$

For Figure 4.1 through Figure 4.3 the initial values of ψ, ϕ, $\dot{\theta}$ and $\dot{\psi}$ are all set to zero. The relevant initial conditions (θ and $\dot{\phi}$) are specified in the caption to each subplot. Some more relevant initial parameters of the disk include:

- $m = 1\ \ (Disk\ mass)$
- $a = 1\ (Disk\ radius)$
- $h = 2\ (Disk\ height)$

- $C = [0.03,\ 0.073,\ 0.185]$ $(Drag\ coefficients)$ (It is worth noting that these drag coefficients imply a grain either in the disk or on the surface holding the disk due to the difference between C_x and C_y which would otherwise be equal)

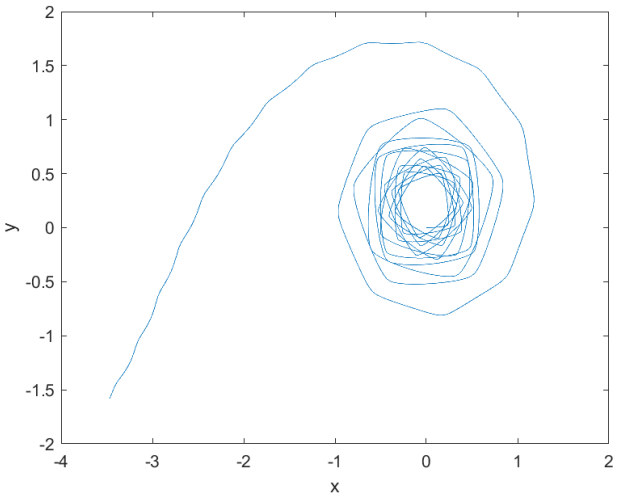

Figure 4.1a: $\theta_{high},\ \dot{\phi}_{high}$

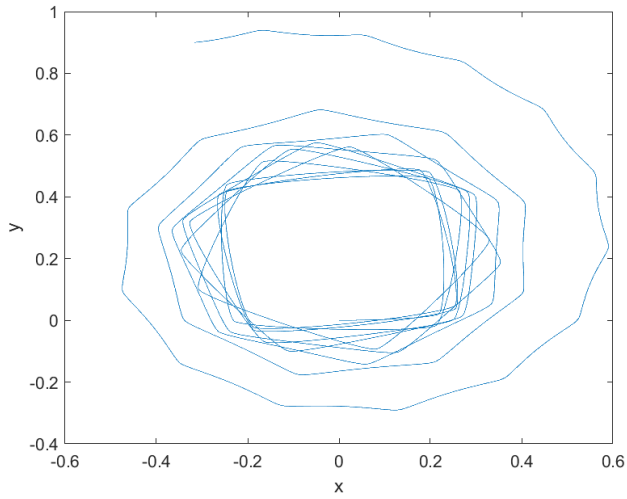

Figure 4.1b: $\theta_{high},\ \dot{\phi}_{low}$

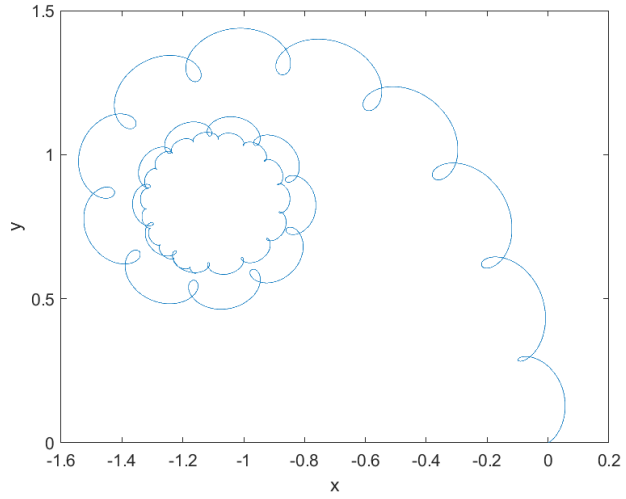

Figure 4.1c: $\theta_{low},\ \dot{\phi}_{high}$

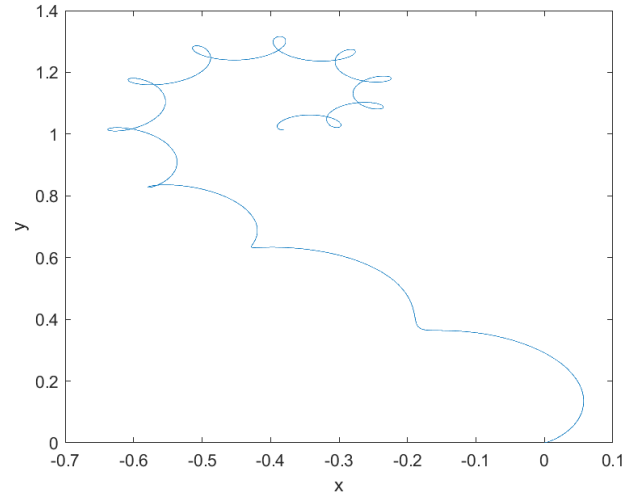

Figure 4.1d: $\theta_{low},\ \dot{\phi}_{low}$

Figure 4.1: Trajectories of centre of mass

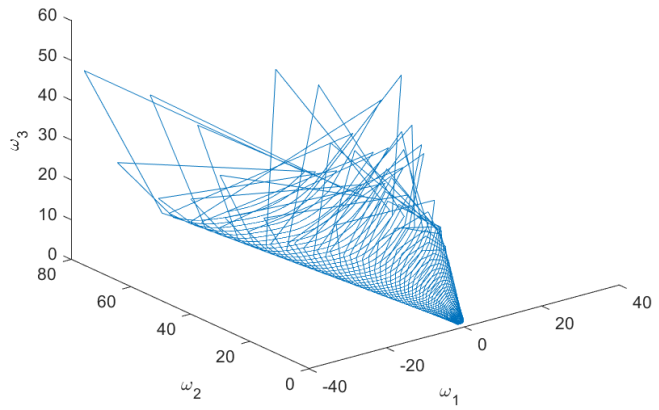

Figure 4.2a: θ_{high}, $\dot{\phi}_{high}$

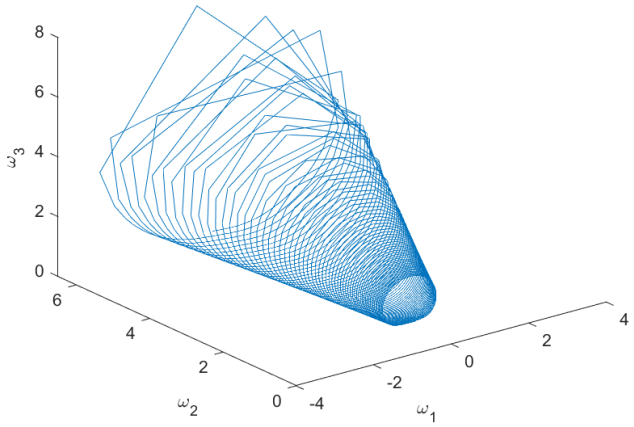

Figure 4.2b: θ_{high}, $\dot{\phi}_{low}$

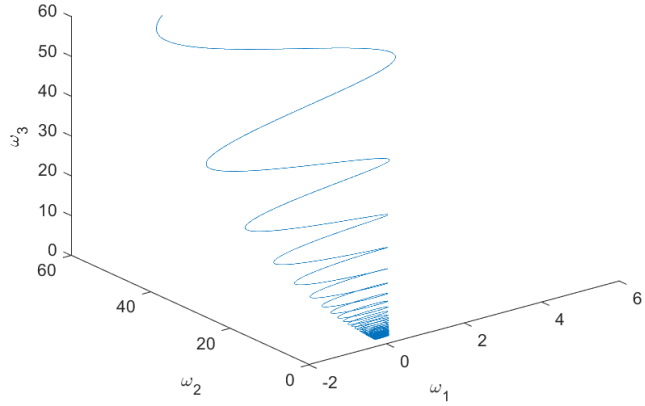

Figure 4.2c: θ_{low}, $\dot{\phi}_{high}$

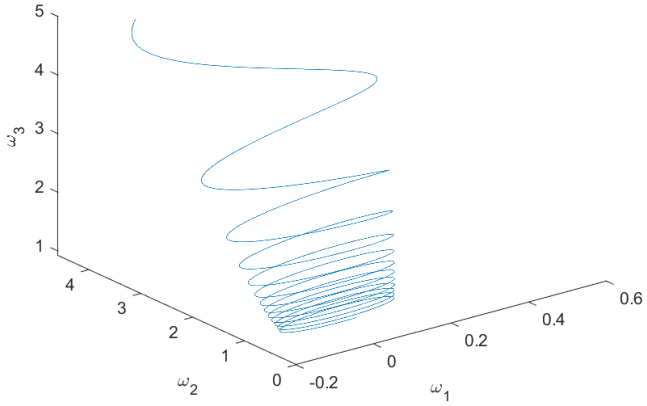

Figure 4.2d: θ_{low}, $\dot{\phi}_{low}$

Figure 4.2: Angular velocity spirals

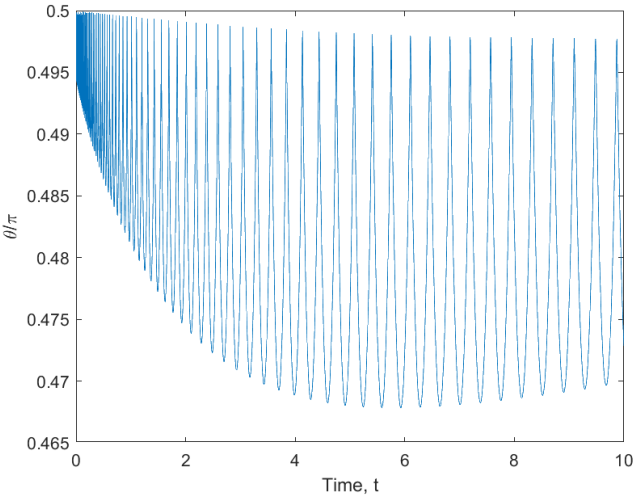

Figure 4.3a: θ_{high}, $\dot{\phi}_{high}$

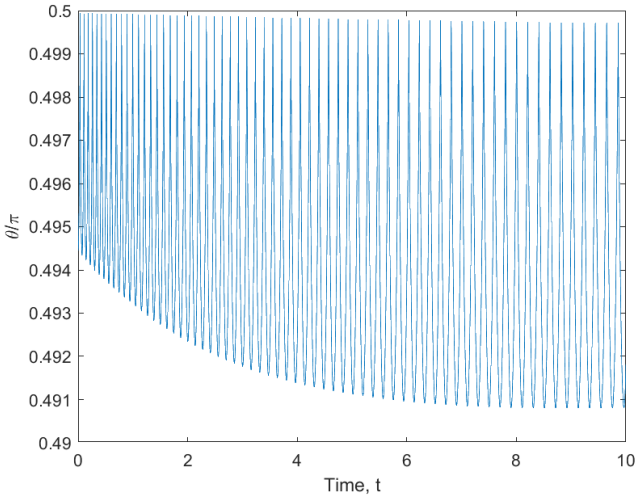

Figure 4.3b: θ_{high}, $\dot{\phi}_{low}$

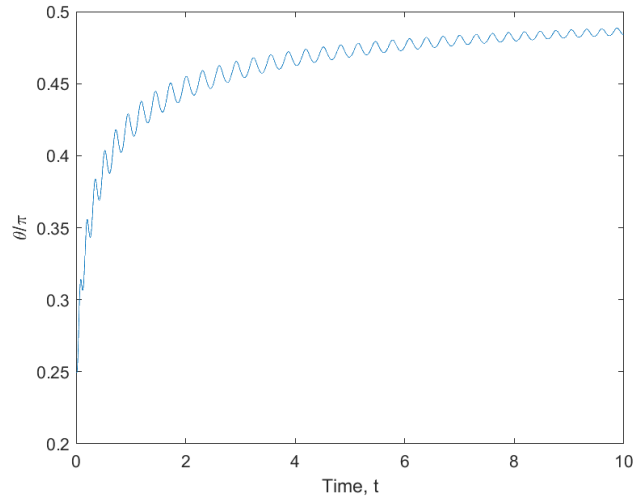

Figure 4.3c: θ_{low}, $\dot{\phi}_{high}$

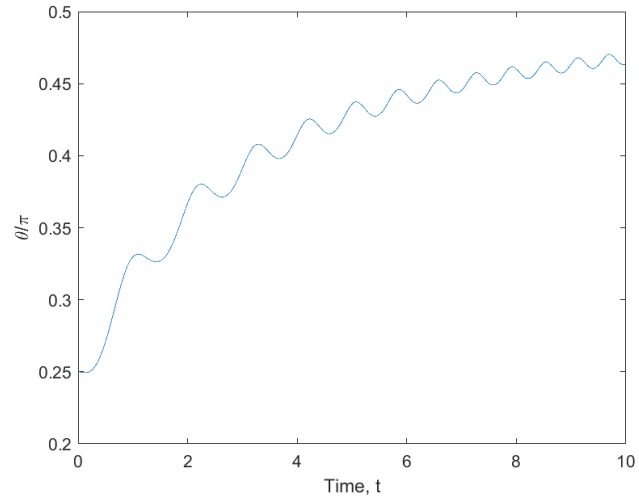

Figure 4.3d: θ_{low}, $\dot{\phi}_{low}$

Figure 4.3: Normalised nutation vs time

4.2. Effect of initial $\dot{\psi}$ on the behaviour along the trajectory

The initial revolution rate $\dot{\psi}$ of the disk has been set to zero thus far. This can however have an interesting effect on the trajectory of the disk. The nutation was set to 89° and the same analysis was performed for combinations of 'high' and 'low' initial values of $\dot{\psi}$ and $\dot{\phi}$. (Figure 4.4 through Figure 4.6)

- $\dot{\psi}_{high} = \dot{\phi}_{high} = 80\, revolutions\, t^{-1}$
- $\dot{\psi}_{low} = \dot{\phi}_{low} = 6.5\, revolutions\, t^{-1}$

The values of m, a, h and C (mass, radius, height and drag coefficients) are identical to those in Section 5.1.

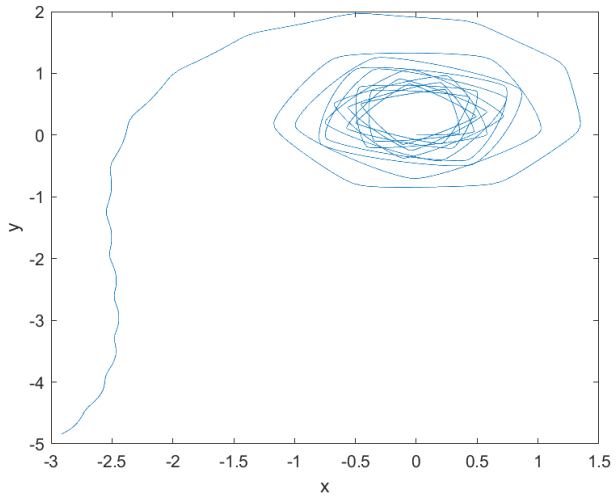

Figure 4.4a: $\dot{\psi}_{high}$, $\dot{\phi}_{high}$

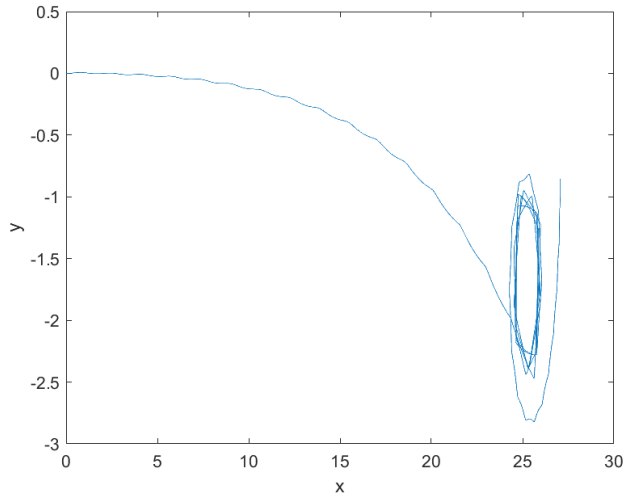

Figure 4.4b: $\dot{\psi}_{high}$, $\dot{\phi}_{low}$

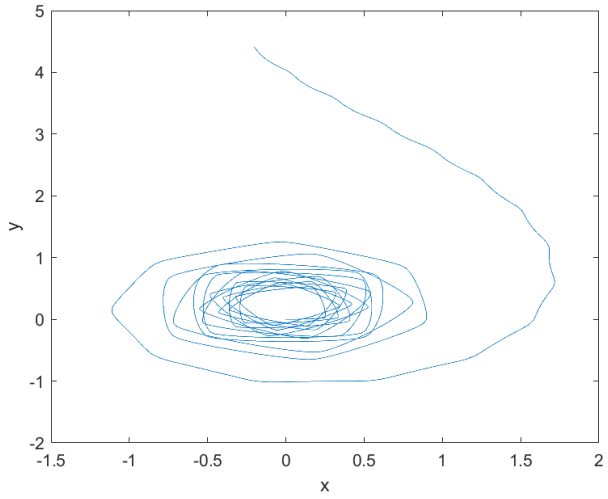

Figure 4.4c: $\dot{\psi}_{low}$, $\dot{\phi}_{high}$

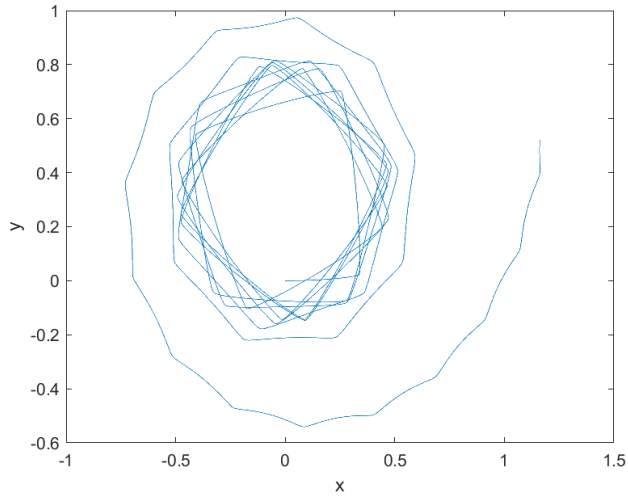

Figure 4.4d: $\dot{\psi}_{low}$, $\dot{\phi}_{low}$

Figure 4.4: Trajectories of centre of mass with nonzero $\dot{\psi}_0$

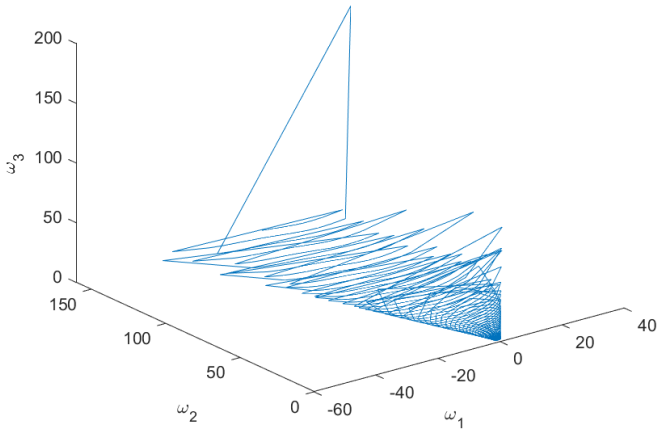

Figure 4.5a: $\dot{\psi}_{high},\ \dot{\phi}_{high}$

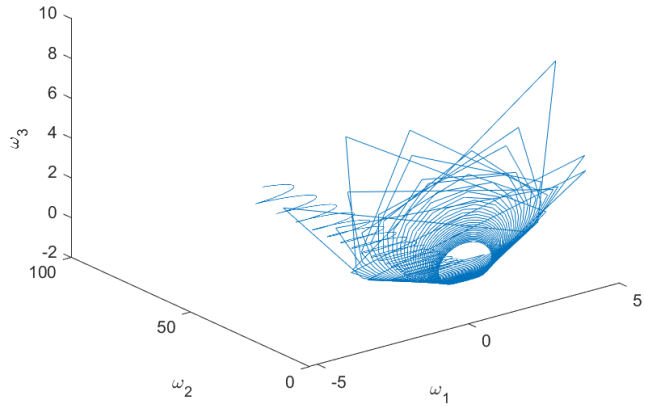

Figure 4.5b: $\dot{\psi}_{high},\ \dot{\phi}_{low}$

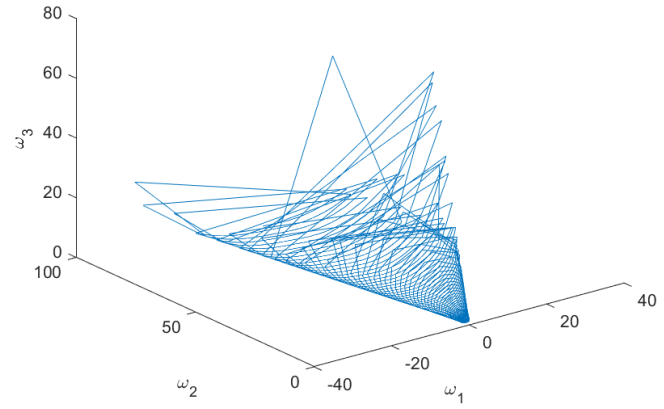

Figure 4.5c: $\dot{\psi}_{low},\ \dot{\phi}_{high}$

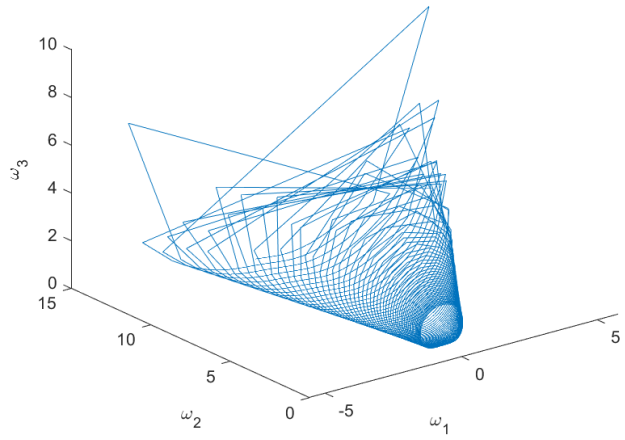

Figure 4.5d: $\dot{\psi}_{low},\ \dot{\phi}_{low}$

Figure 4.5: Angular velocity spirals with nonzero $\dot{\psi}_0$

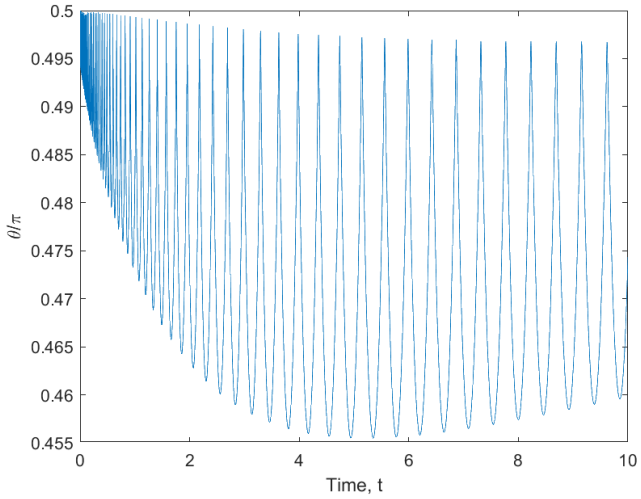

Figure 4.6a: $\dot{\psi}_{high},\ \dot{\phi}_{high}$

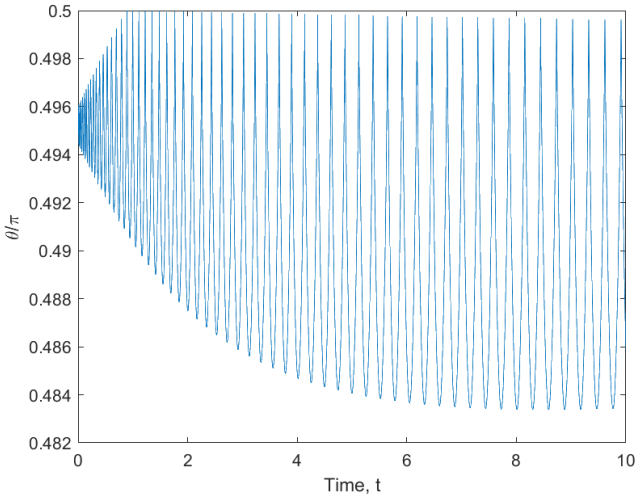

Figure 4.6b: $\dot{\psi}_{high},\ \dot{\phi}_{low}$

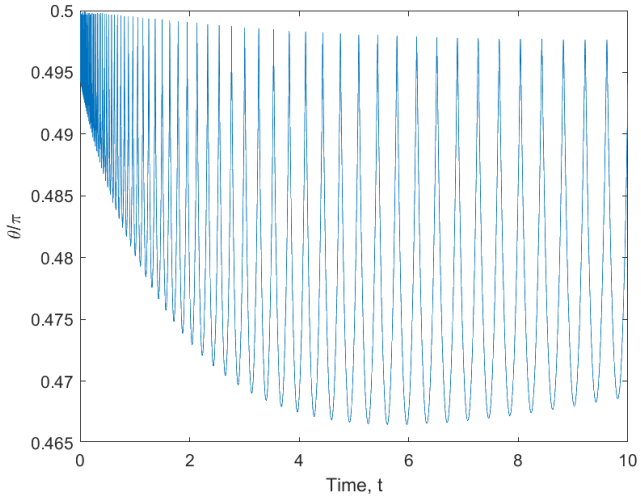

Figure 4.6c: $\dot{\psi}_{low},\ \dot{\phi}_{high}$

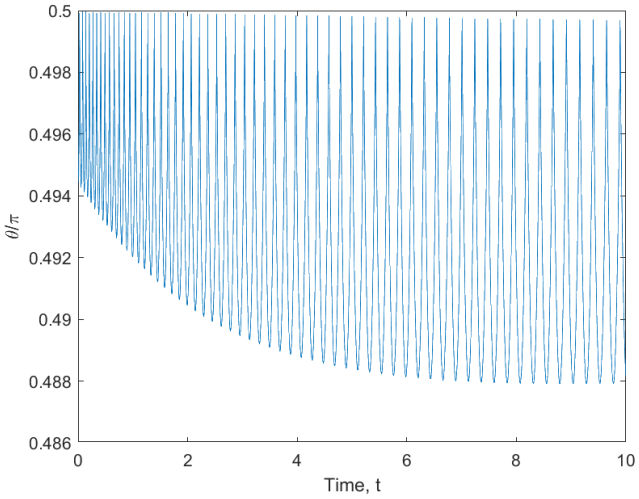

Figure 4.6d: $\dot{\psi}_{low},\ \dot{\phi}_{low}$

Figure 4.6: Normalised nutation vs time with nonzero $\dot{\psi}_0$

4.3.Lyapunov exponents due to variation in initial nutation

Using the model and the background theory detailed previously (Equation 1.15), it is assumed that the absolute distance between the trajectories of the centre of mass at slightly different initial nutations increases roughly exponentially as time progresses. Using this theory, the log of this distance is plotted against time and a roughly straight line should

result. The slope of this line should be equal to the Lyapunov exponent. These plots of $\ln(d_t)$ vs t can be generated for many different sets of slightly varying values of θ_0, for instance:

- $\theta_{0_1} = 40°,\ \theta_{0_2} = 39.999°$
- $\theta_{0_1} = 60°,\ \theta_{0_2} = 59.999°$

This is carried out for all values of θ_{0_1} from 28° to 89° in increments of 1° with the slightly varied value $\theta_{0_2} = \theta_{0_1} - 0.001$. The resultant plots are too numerous and the differences between them too gradual to include all of them in this report. The behaviour is instead summarised by showing the graphs in increments of 10° (i.e. $29°, 39°, \dots, 89°$). The full list of images is also available on GitHub. [6]

A suitable range of points needs to be chosen for each plot in order to calculate the Lyapunov exponent at the corresponding nutation. This involves taking the slope of the line of best fit of a region near the beginning of the plot. The location of this range is highly subjective (as shown in Figure 4.7) and highly error prone. It is highly likely that the approximation of the distance between the centre of mass trajectories as exponentially increasing is inaccurate. However, the analysis can still be carried out for a relatively narrow range of datapoints to gain an understanding of the variation of λ with nutation. Due to the high sensitivity of the slope of the graph depending on the range of points chosen, the same region of the graph must be analysed for all values of θ. The range chosen for this project was the highly linear region immediately after the first local minimum e.g.

- $\theta_0 = 29° \rightarrow range\ begins\ @t \approx 0.04$ (Figure 4.7a)
- $\theta_0 = 69° \rightarrow range\ begins\ @t \approx 0.07$ (Figure 4.7e)

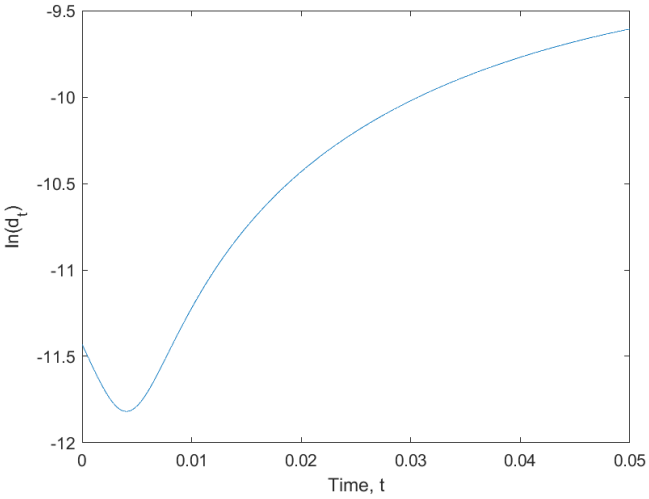

Figure 4.7a: $\theta_0 = 29°$

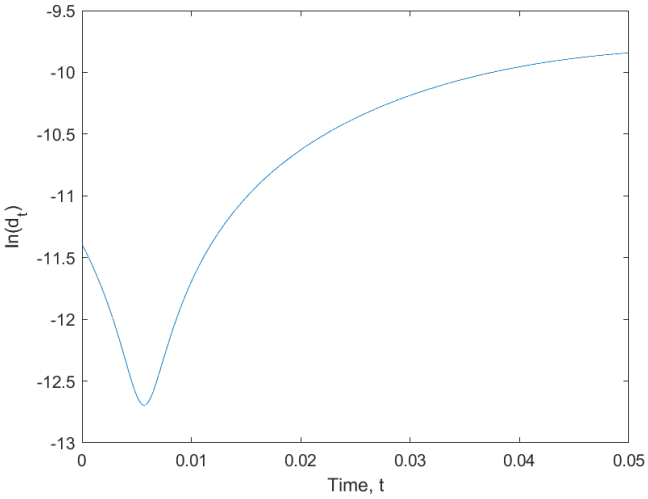

Figure 4.7b: $\theta_0 = 39°$

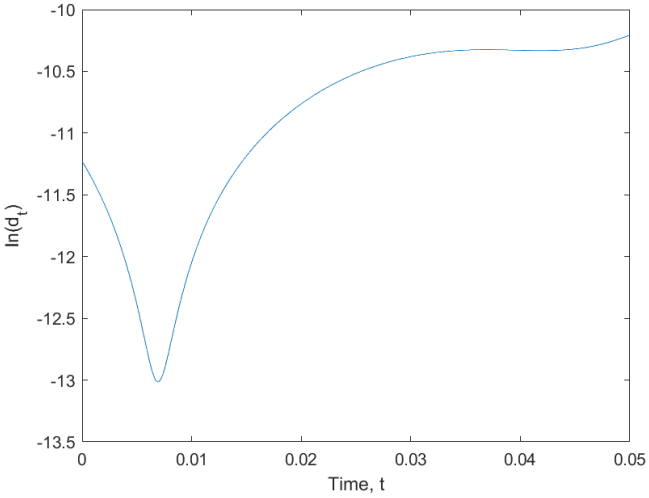

Figure 4.7c: $\theta_0 = 49°$

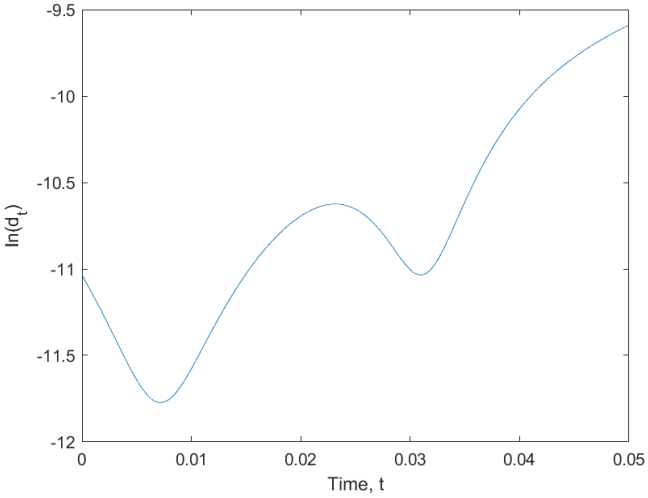

Figure 4.7d: $\theta_0 = 59°$

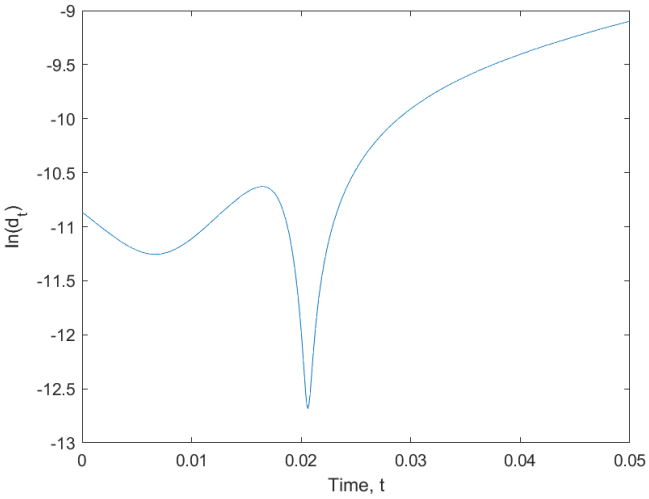

Figure 4.7e: $\theta_0 = 69°$

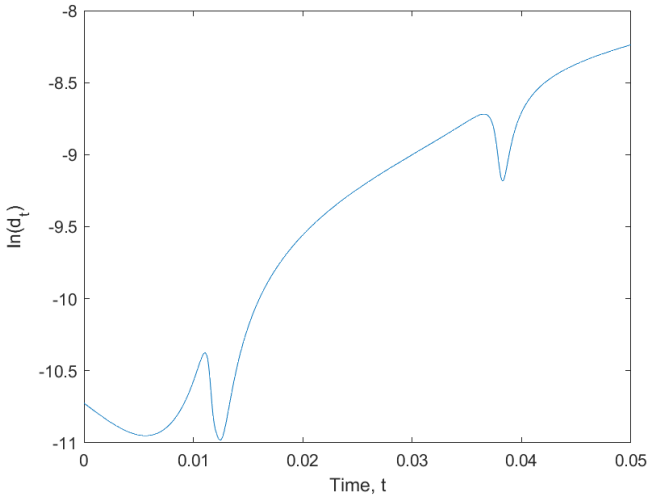

Figure 4.7f: $\theta_0 = 79°$

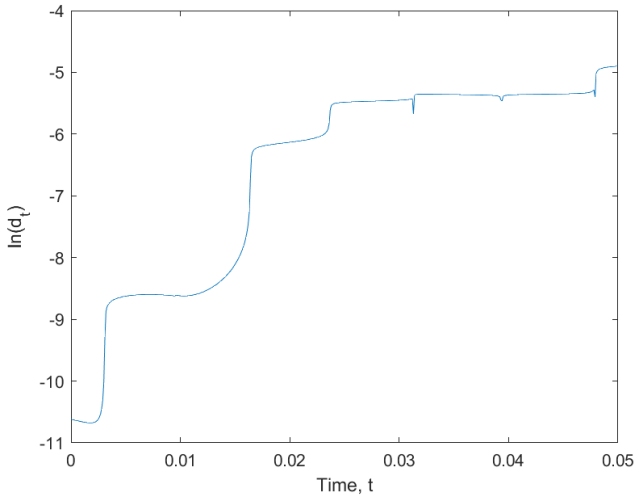

Figure 4.7g: $\theta_0 = 89°$

Figure 4.7: $ln\ (d_t)$ vs t relationships at varying θ_0

The values of m, a, h and C again remain unchanged

4.4. Variation of the drag between the disk and the surface

The drag coefficients between the disk and the surface have so far remained unchanged throughout the project. These may be varied to determine the behaviour of the disk under various frictional conditions. The exact values selected for the drag coefficients, C are

arbitrary (the values selected thus far throughout the project have been $[0.03,\ 0.073, 0.185]$) however one could determine from the equations involved what is the implicit unit of the drag coefficients (which assuming SI units would be unitless). The extent of this study is simply to show the behaviour of the disk with respect to the relative size of the drag coefficients rather than to measure the exact units involved in the drag coefficient. It is perhaps more productive to look at the drag in the xy-plane and along the z-axis separately. The initial nutation $\theta_0 = 89°$ and the initial precession rate $\dot{\phi}_0 = 80$.

First, we look at the drag coefficients in the xy-plane with $C_z = 0.185$ as in previous sections

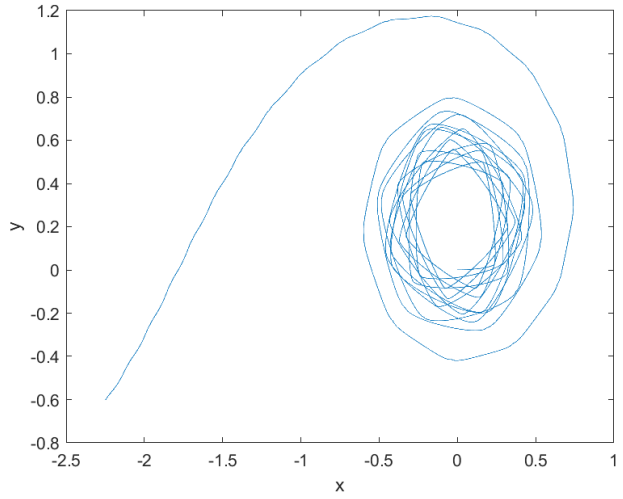

Figure 4.8a: $C_x = C_y = 0.1$

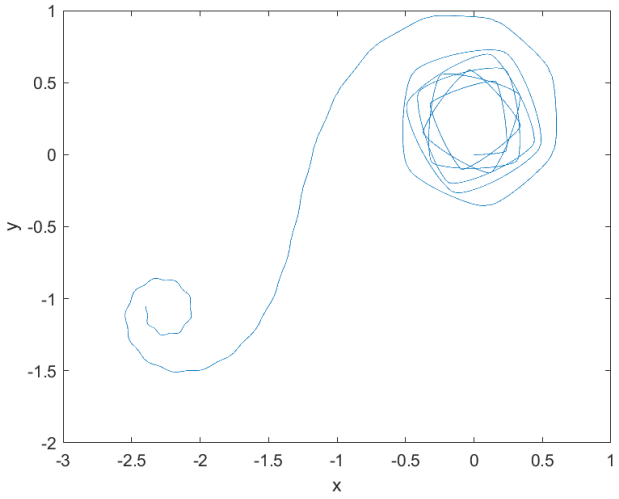

Figure 4.8b: $C_x = C_y = 0.2$

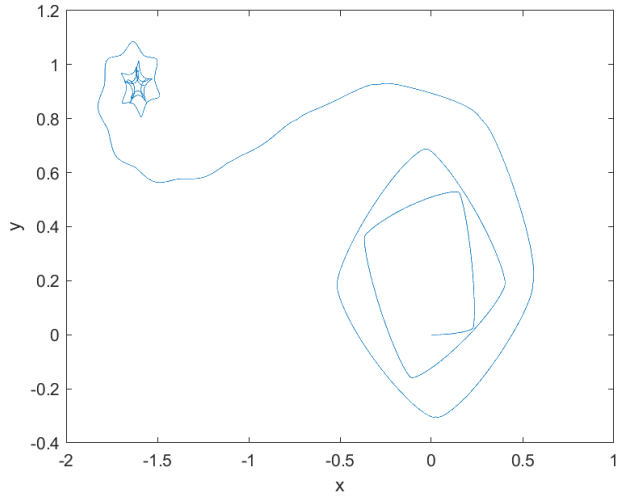

Figure 4.8c: $C_x = C_y = 0.5$

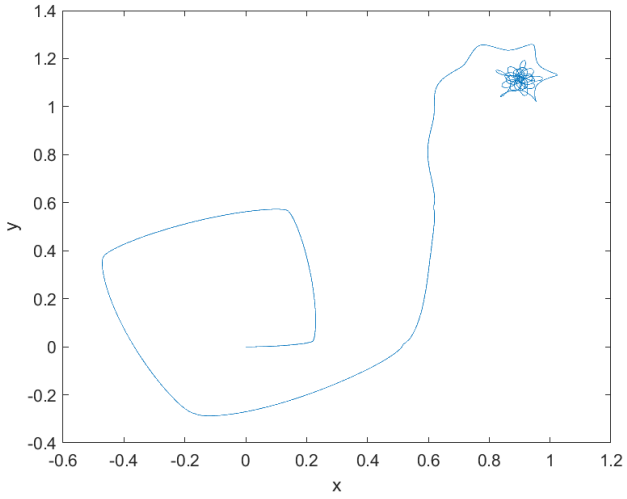

Figure 4.8d: $C_x = C_y = 1$

Figure 4.8: Trajectories of centre of mass with varying xy-plane drag

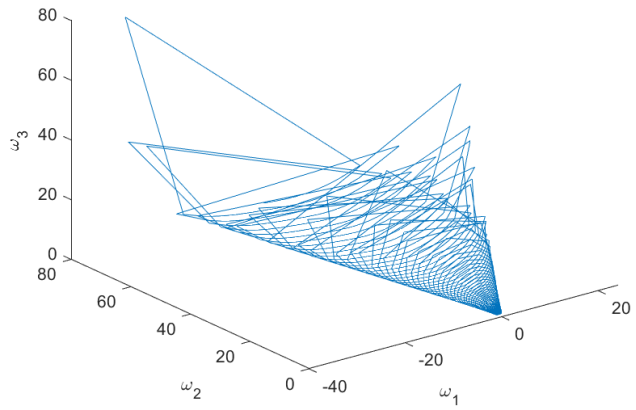

Figure 4.9a: $C_x = C_y = 0.1$

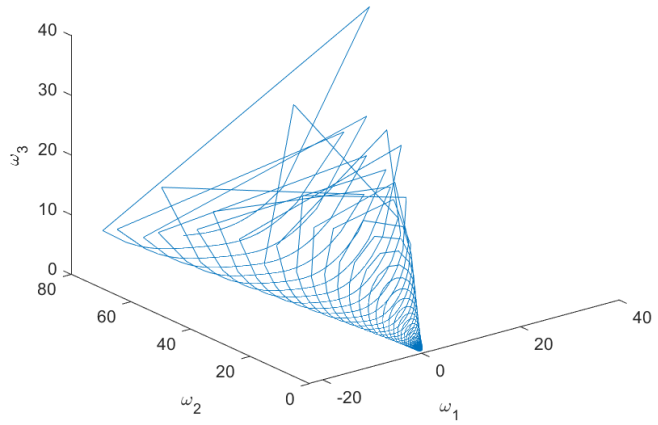

Figure 4.9b: $C_x = C_y = 0.2$

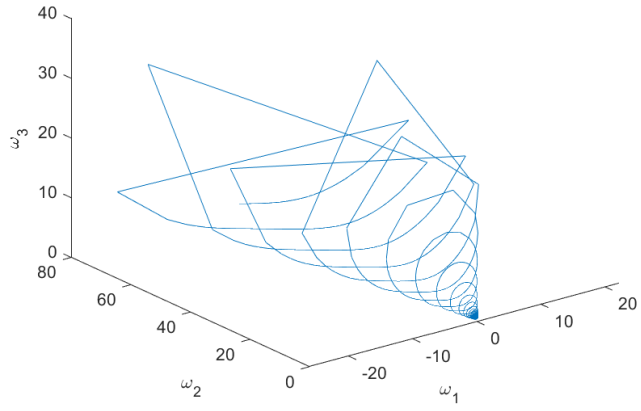

Figure 4.9c: $C_x = C_y = 0.5$

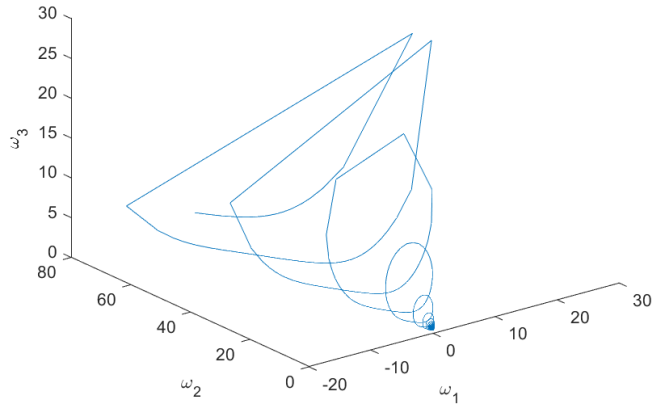

Figure 4.9d: $C_x = C_y = 1$

Figure 4.9: Angular velocity spirals with varying xy-plane drag

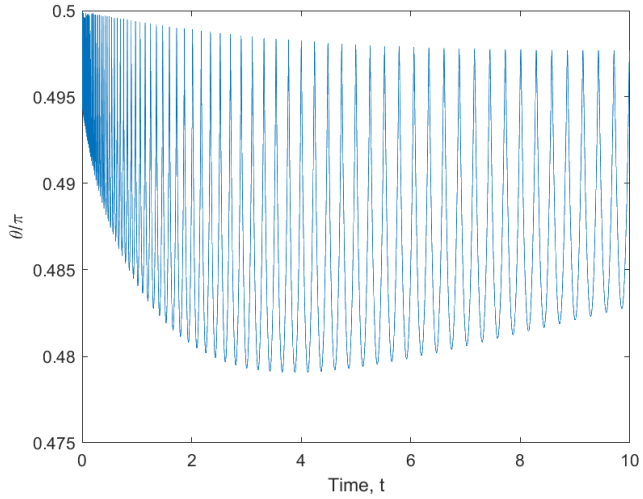

Figure 4.10a: $C_x = C_y = 0.1$

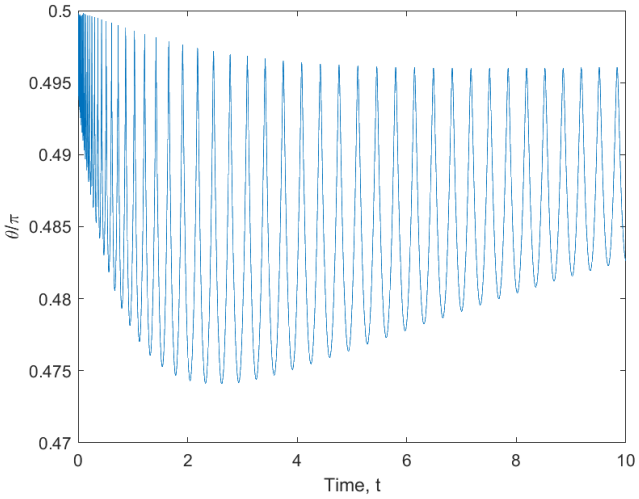

Figure 4.10b: $C_x = C_y = 0.2$

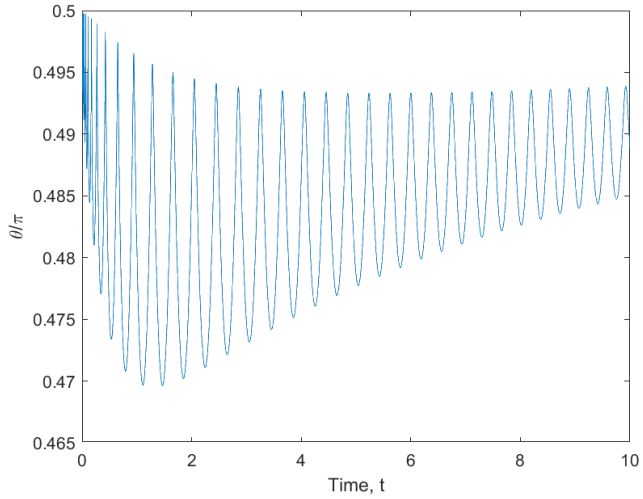

Figure 4.10c: $C_x = C_y = 0.5$

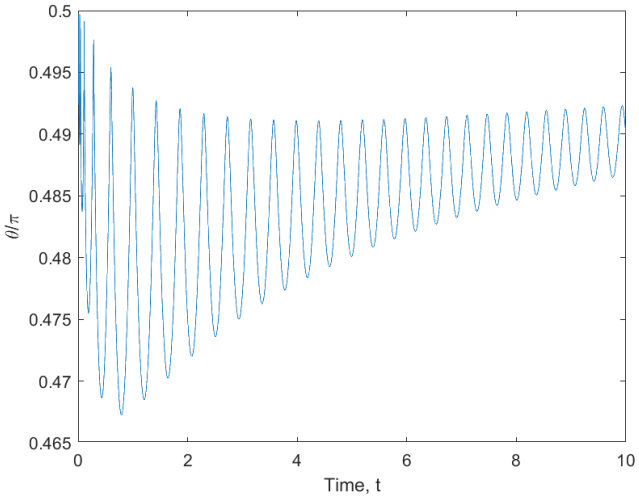

Figure 4.10d: $C_x = C_y = 1$

Figure 4.10: Evolution of normalised nutation with varying xy-plane drag

We can also analyse the effect of drag in the z-direction on the trajectory with $C_x = C_y = 0.1$.

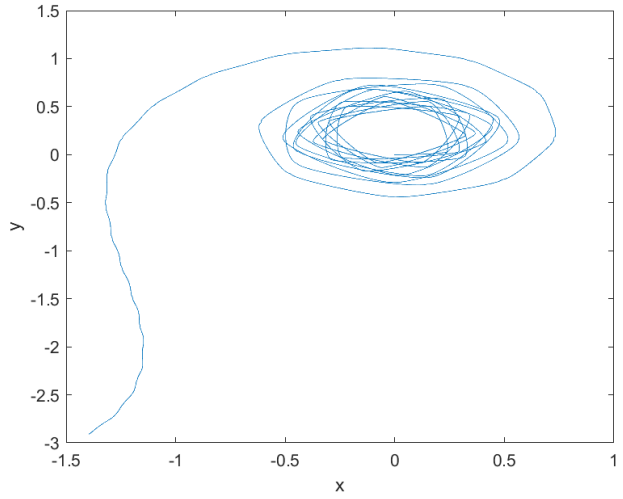

Figure 4.11a: $C_z = 0.1$

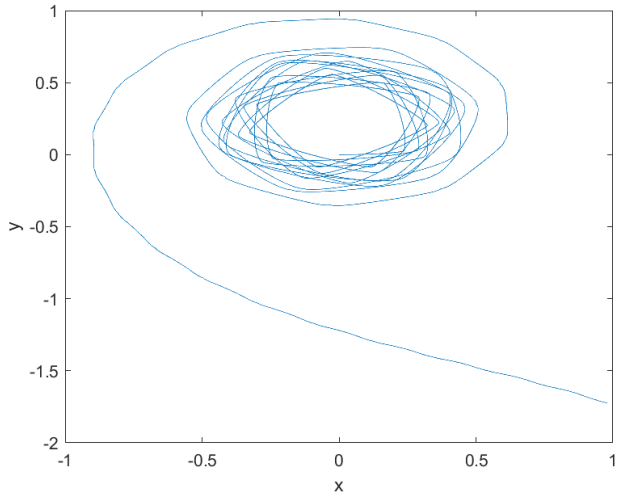

Figure 4.11b: $C_z = 0.2$

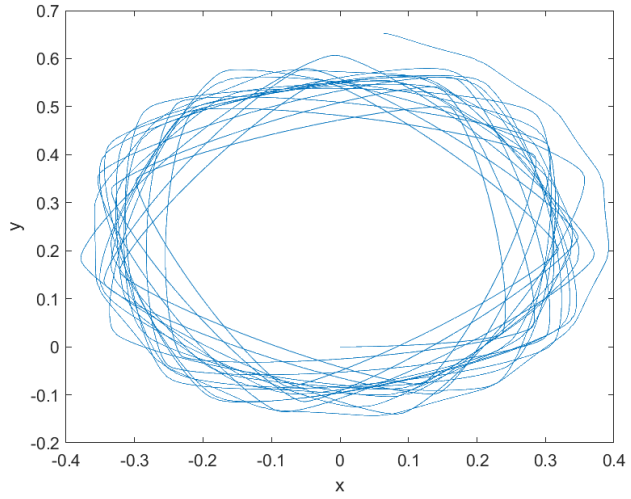

Figure 4.11c: $C_z = 0.5$

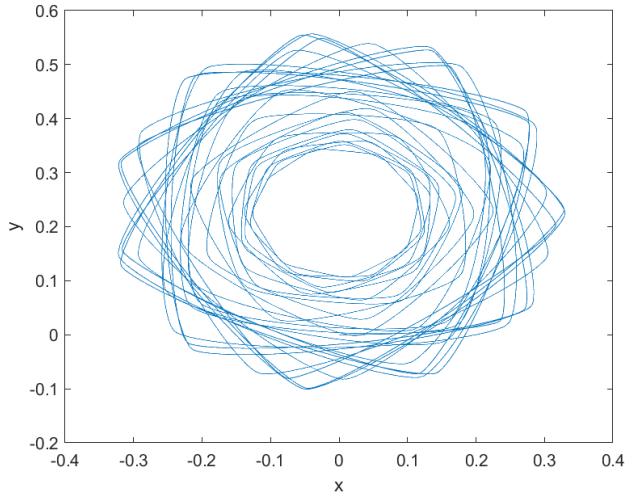

Figure 4.11d: $C_z = 1$

Figure 4.11: Trajectories of centre of mass with varying C_z

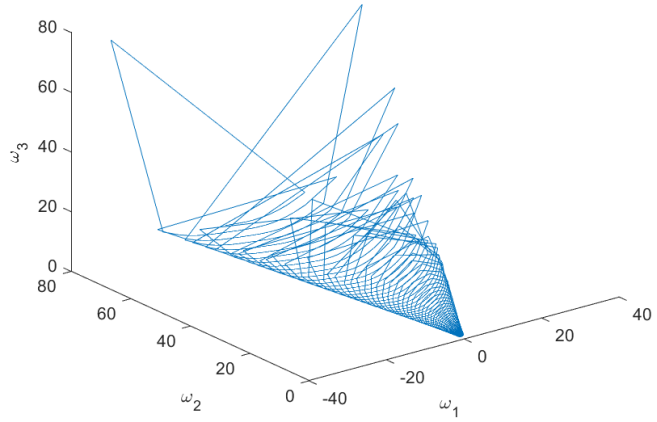

Figure 4.12a: $C_z = 0.1$

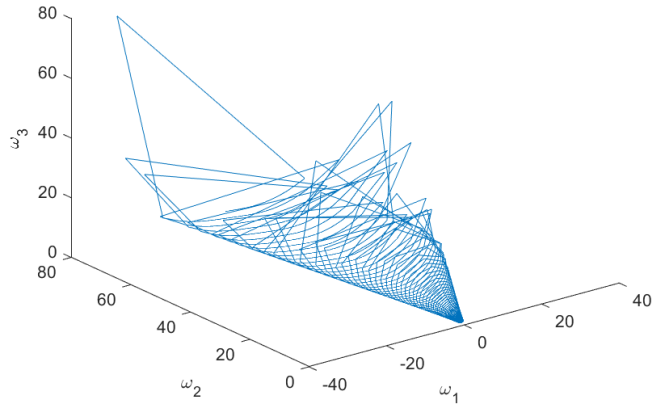

Figure 4.12b: $C_z = 0.2$

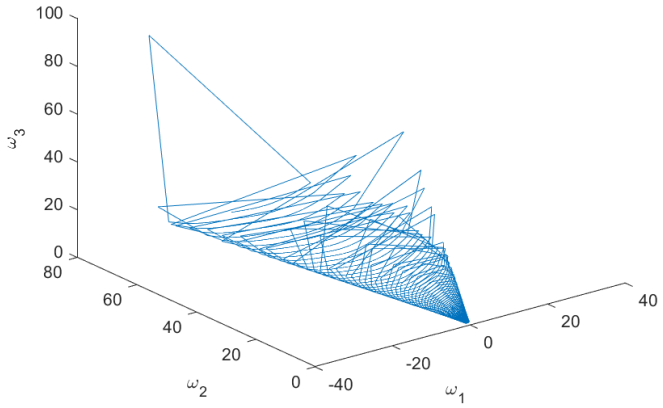

Figure 4.12c: $C_z = 0.5$

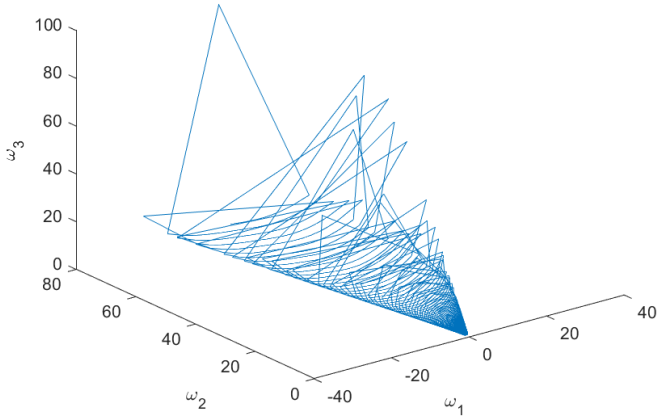

Figure 4.12d: $C_z = 1$

Figure 4.12: Angular velocity spirals with varying C_z

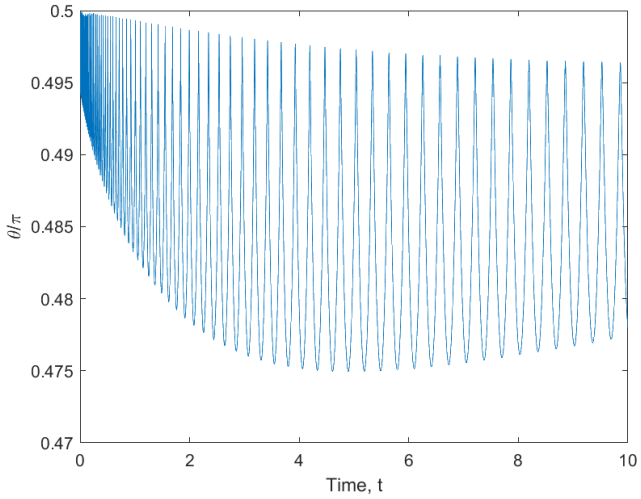

Figure 4.13a: $C_z = 0.1$

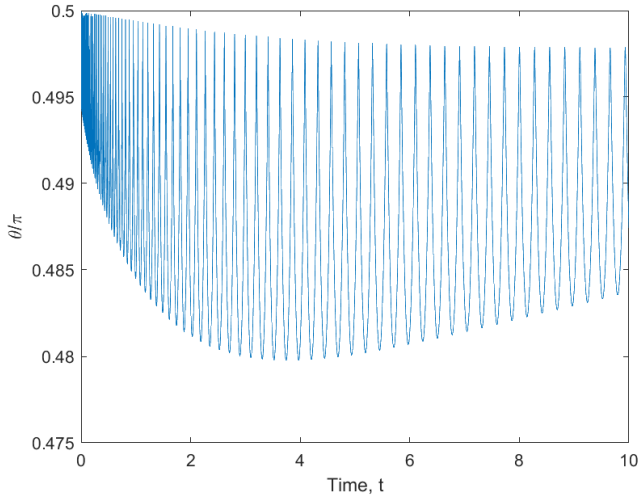

Figure 4.13b: $C_z = 0.2$

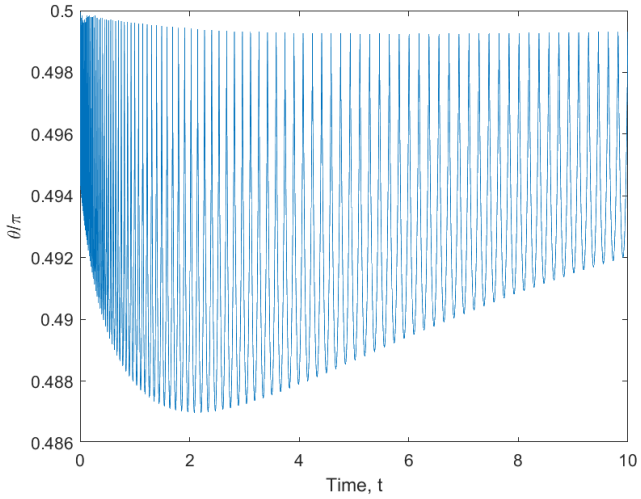

Figure 4.13c: $C_z = 0.5$

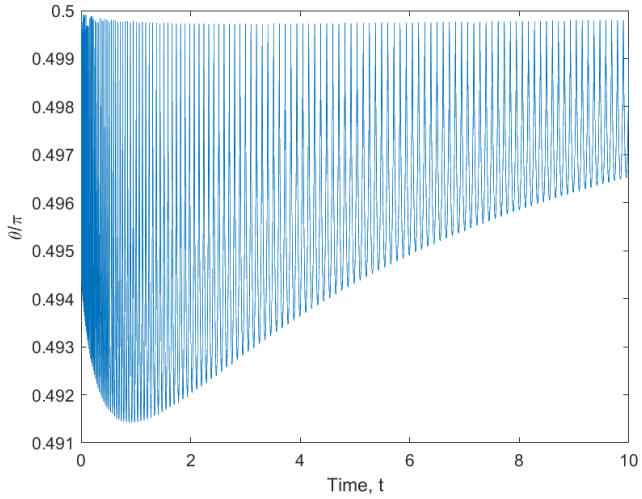

Figure 4.13d: $C_z = 1$

Figure 4.13: Evolution of normalised nutation with varying C_z

4.5. Calculating the Lyapunov exponents vs θ_0

This range of datapoints, as described earlier, was difficult to automate for all θ. The LE was therefore calculated manually (Table 7.1). The values are then expressed relative to λ_{min} (Table 7.2). These data tables are illustrated in the appendix.

The data in Table 7.2 is illustrated in **Error! Reference source not found.**a and again in REF _Ref37353152 \h * MERGEFORMAT **Error! Reference source not found.**b but

without the last eight datapoints to more easily visualise the relationship for the bulk of the plot.

The values of m, a, h and C again remain unchanged and the rate of precession was set unperturbed at $\dot{\phi} = 80\ revolutions\ t^{-1}$ (No revolution $\dot{\psi}$).

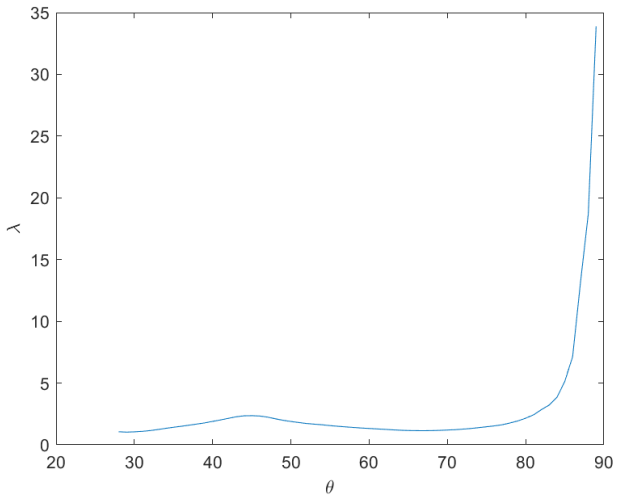

Figure 4.14a: Entire relationship (smoothed plot)

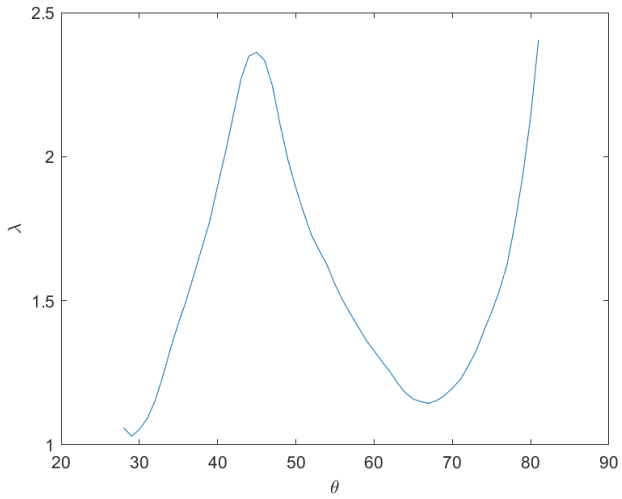

Figure 4.14b: $\theta_0 = 28° \rightarrow 81°$ (smoothed plot)

Figure 4.14: Relative Lyapunov exponent vs initial nutation

The three notable points in **Error! Reference source not found.**b are the local minima at $\theta = 30°, 66°$ and the local maximum at $\theta = 45°$. These points may be further analysed by looking at the trajectories of the centre of mass around $\theta = 30°, 45°$.

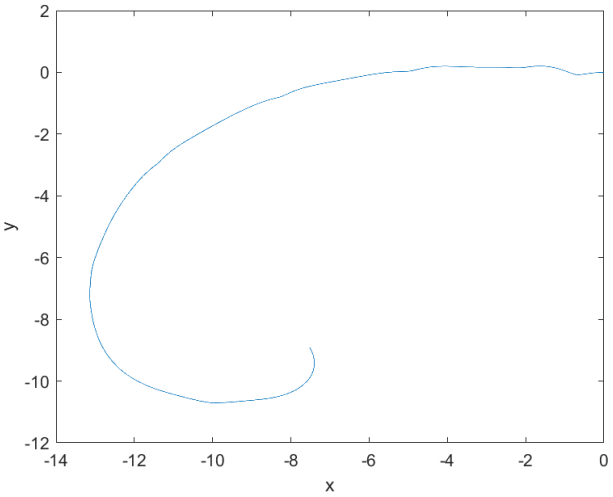

Figure 4.15a: $\theta = 31°$ ($t_{max} = 6.99$)

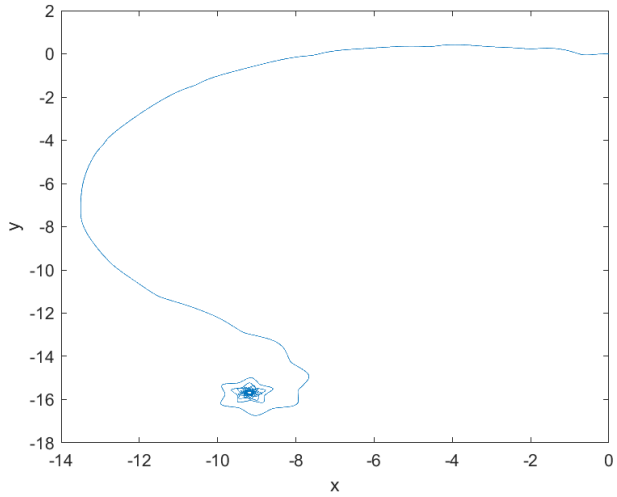

Figure 4.15b: $\theta = 32°$

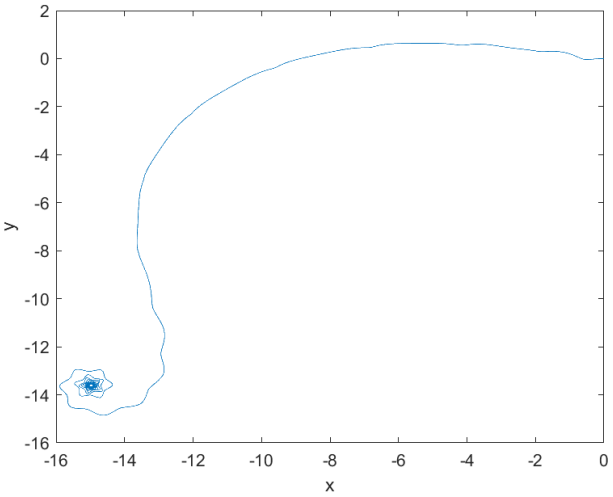

Figure 4.15c: $\theta = 33°$

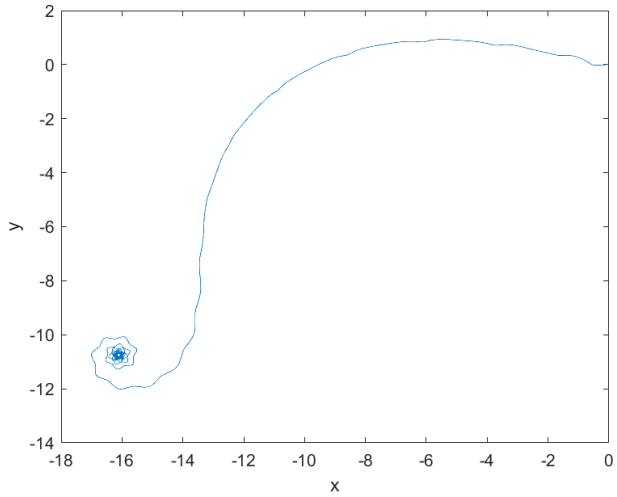

Figure 4.15d: $\theta = 34°$

Figure 4.15: Centre of mass trajectories from $t = 0$ to $t = 50$ (unless otherwise specified) for $\theta \to 30°$

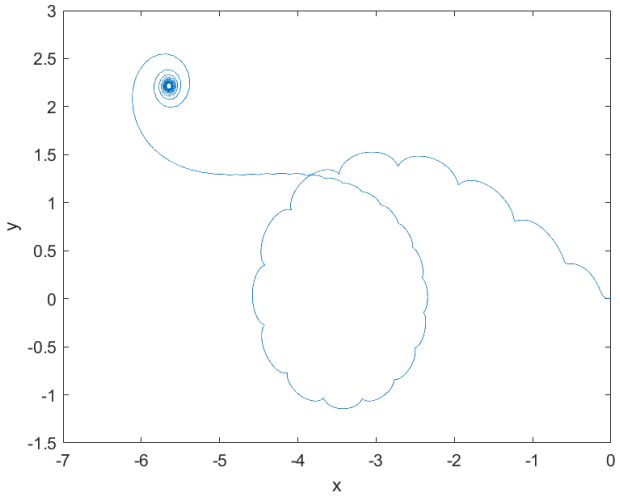

Figure 4.16a: $\theta = 41°$

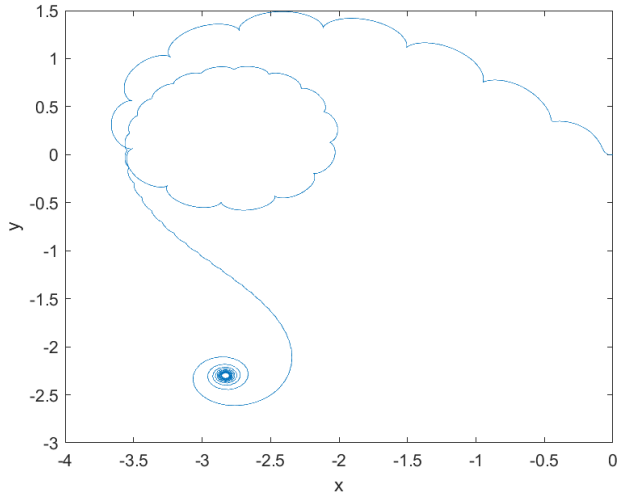

Figure 4.16b: $\theta = 42°$

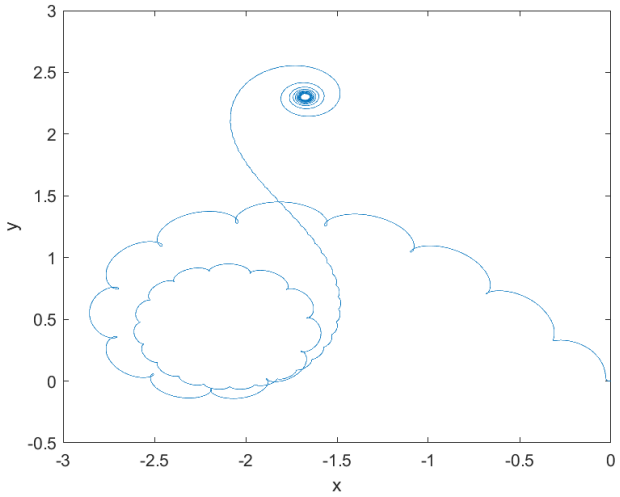

Figure 4.16c: $\theta = 43°$

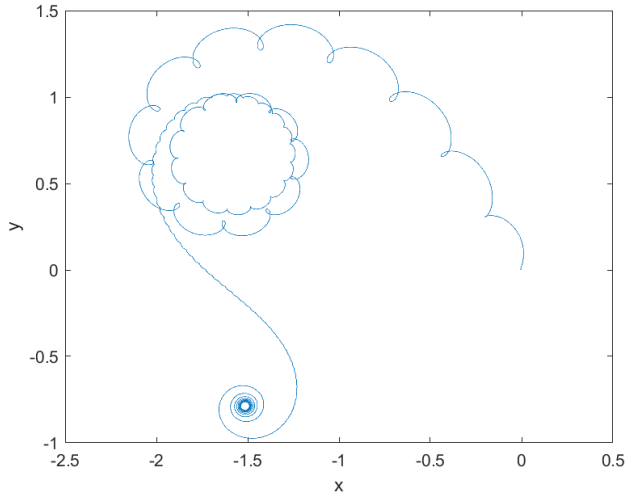

Figure 4.16d: $\theta = 44°$

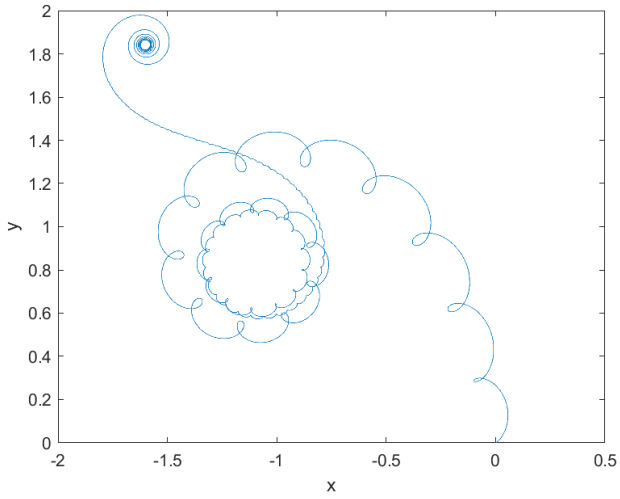

Figure 4.16e: $\theta = 45°$

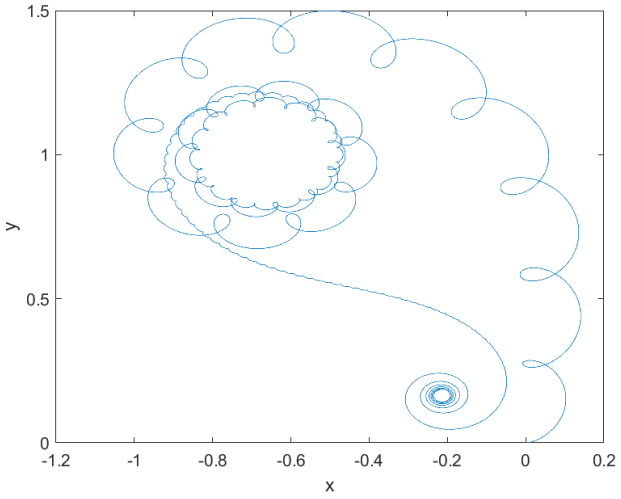

Figure 4.16f: $\theta = 46°$

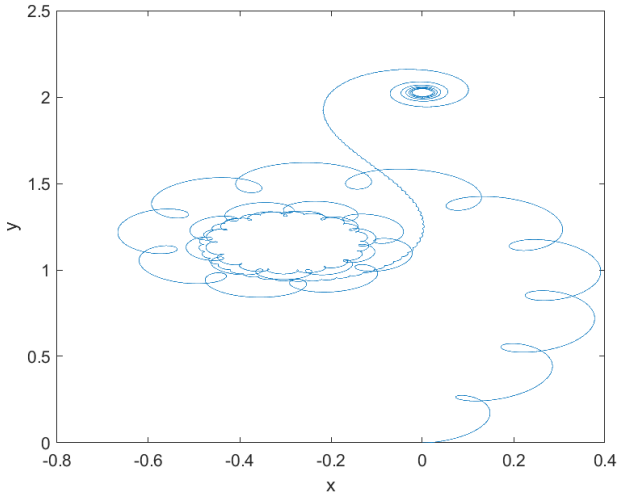

Figure 4.16g: $\theta = 47°$

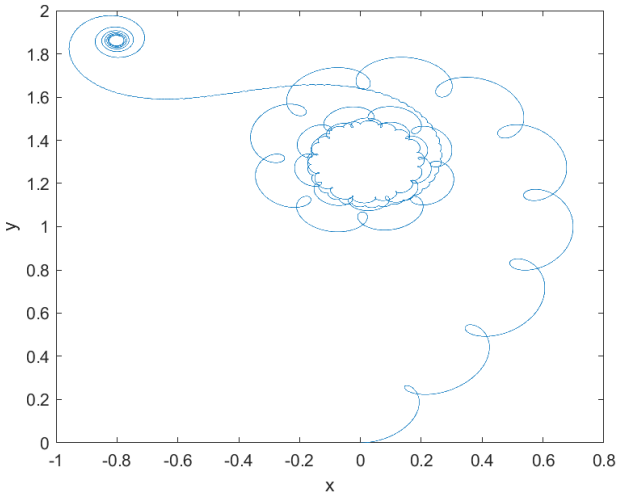

Figure 4.16h $\theta = 48°$

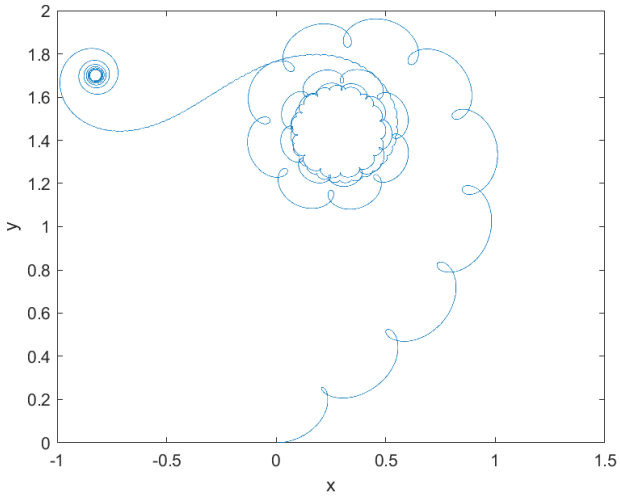

Figure 4.16i: $\theta = 49°$

Figure 4.16: Centre of mass trajectories from $t = 0$ *to* $t = 50$ *for* $\theta \to 45°$

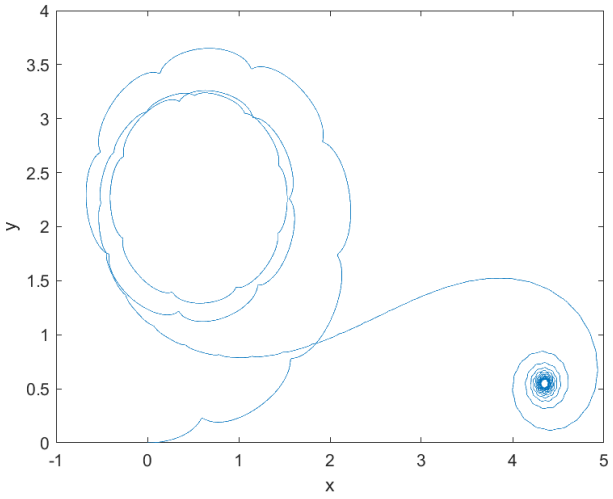

Figure 4.17a: $\theta = 62°$

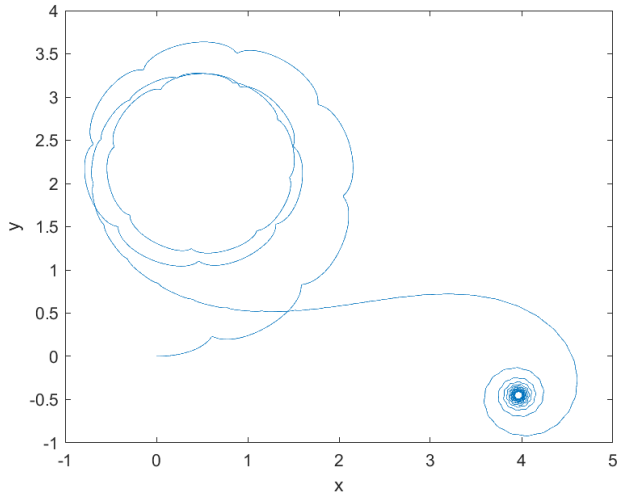

Figure 4.17b: $\theta = 63°$

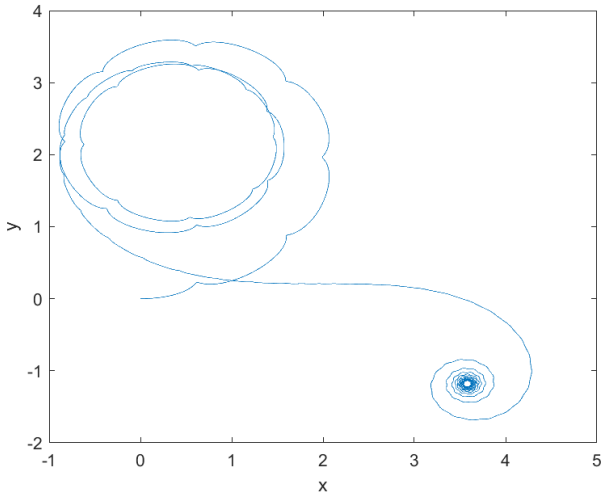

Figure 4.17c: $\theta = 64°$

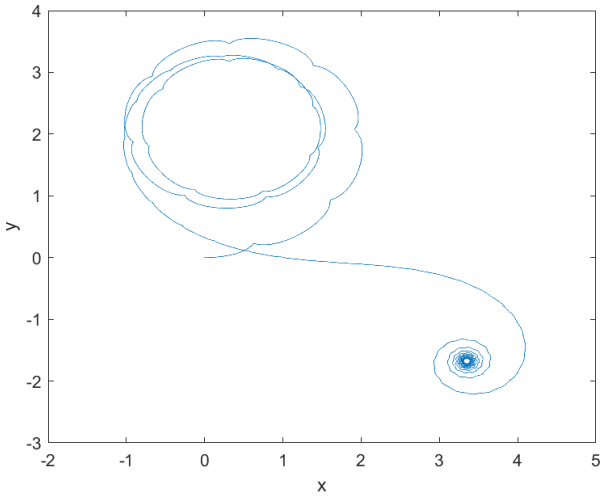

Figure 4.17d: $\theta = 65°$

Figure 4.17: Centre of mass trajectories from $t = 0$ to $t = 50$ for $\theta \to 66°$

5. Interpretation and Discussion

5.1. The path of the COM in the xy-plane

The effect of the initial conditions on the path of the centre of mass of the disk is illustrated in Figure 4.1, Figure 4.4, Figure 4.8 and Figure 4.11. Looking at the axes of the four plots in Figure 4.1, it is clear that the distance across which the centre of mass travels is maximised when the initial nutation and initial rate of precession are both high whereas

when either θ_0 or $\dot{\phi}_0$ are low, the disk is not able to travel as far. It is also observed that the disk undergoes far less 'orbiting' behaviour when the initial nutation is low, displaying instead a more unstable 'rocking' motion indicated by the frequent looping of the centre of mass along the trajectory.

From Figure 4.4 it is clear that, again, the disk tends to travel significantly further when a high revolution rate $(\dot{\psi})$ is combined with the regular precession motion (comparing 5.4a and 5.4b with 5.4c and 5.4d). A more potentially surprising result is the fact that the disk travelled significantly further when a high rate of revolution was combined with a low rate of precession as opposed to when both rates were high. While initially unintuitive, this makes sense as the high rate of precession can work to nullify the effect of the high revolution rate. When this precession is lessened however, the revolution tends to be more dominant which may cause the disk to roll a large distance before the precessive motion takes over.

Looking at Figure 4.8 and Figure 4.11, it is clear that the behaviour of the disk with changing C_x and C_y is highly different from the behaviour as C_z is changed. As the drag on the xy-plane is increased, the disk appears to undergo less initial orbiting and falls into the more linear motion towards the end of the trajectory sooner. However, as the drag along the z-axis is increased, the opposite effect is observed. The disk undergoes far more orbiting as the effect of C_z rises.

5.2. The evolution of the disk's angular velocity

The evolution of the angular velocity vectors are visualised in Figure 4.2, Figure 4.5, Figure 4.9 and Figure 4.12. Some useful ways of qualitatively analysing these plots include

looking at how 'pointed' the end section is (which indicates how quickly the rate of nutation slows**)** and the concentration of the spirals along the ω_2 axis (which indicates the initial damping of the system). These qualities are apparent in Figure 4.2 and Figure 4.5 where a high initial precession appears to have the effect of making ω_1 approach zero faster. Given that $\omega_1 = \dot{\theta}$, this makes sense as it corresponds to the physical tendency of the disk's nutation to stop changing and remain almost upright while the disk is precessing. From Figure 4.5, there are no immediately clear conclusions about the effect of a high rate of revolution on the angular velocity. For the sake of clarity, these plots can be viewed from the top down (ω_1 vs ω_2) to more clearly show the relationships involved (as in Figure 5.1). It is clearer from this view that the angular velocity of the disk is far more sensitive to changes in the precession rate when the revolution rate is high. From Figure 4.9, it appears that the $\vec{\boldsymbol{\omega}}$ spirals become more concentrated as the drag in the xy-plane is increased (indicating that the initial damping of the system is larger) which is to be expected. However, changing the drag in the z-direction appears to have little to no effect on the evolution of the angular velocity (Figure 4.12).

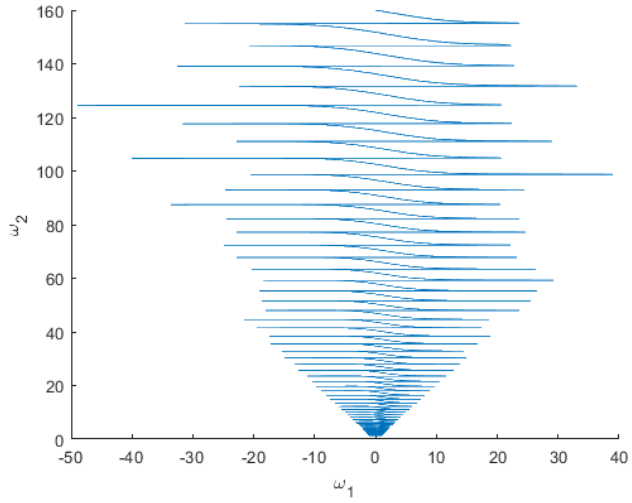

Figure 5.0a: $\dot{\psi}_{high}$, $\dot{\phi}_{high}$

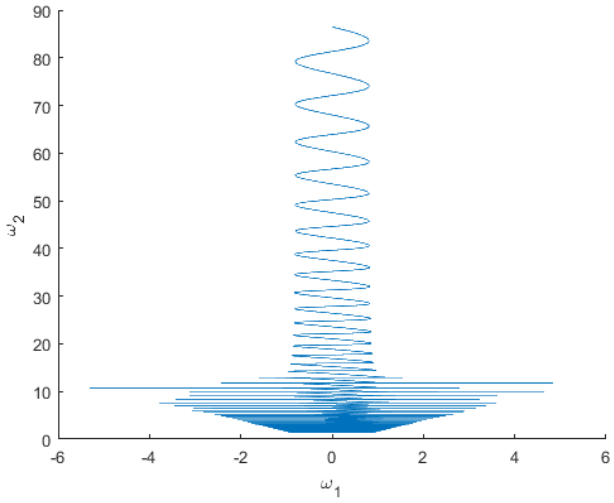

Figure 5.0b: $\dot{\psi}_{high}$, $\dot{\phi}_{low}$

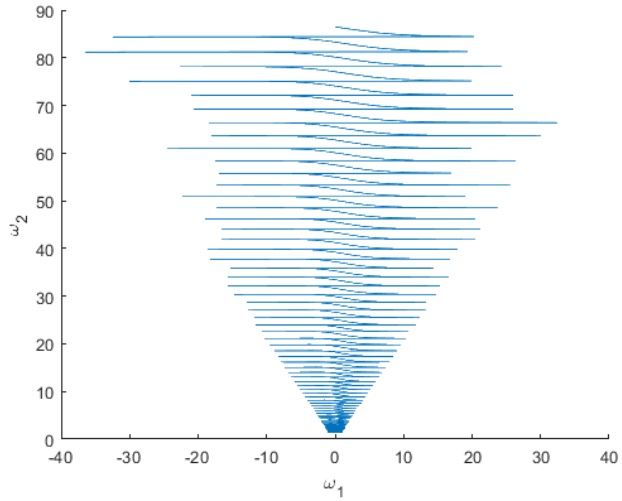

Figure 5.0d: $\dot{\psi}_{low}$, $\dot{\phi}_{high}$

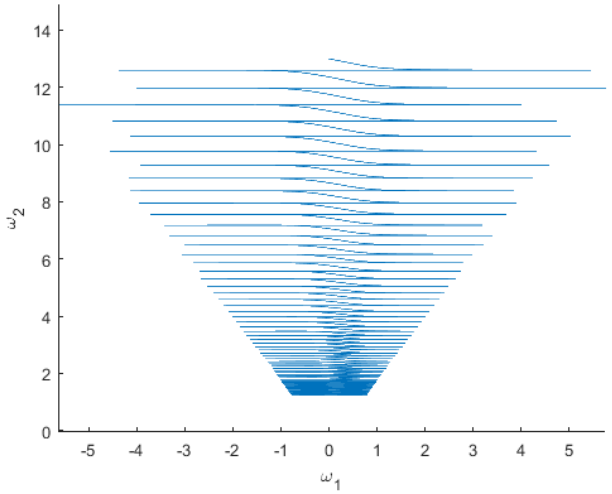

Figure 5.0c: $\dot{\psi}_{low}$, $\dot{\phi}_{low}$

Figure 5.1: ω_1 vs ω_2 with nonzero $\dot{\psi}_0$

5.3. The evolution of the disk's nutation

Figure 4.3 indicates that the initial nutation appears to be proportional to the frequency of oscillation of θ throughout the motion as well as the range of oscillation. This can be expected due to the fact that the disk will tend to align itself at a high nutation shortly after being spun at a low initial nutation. This also shows an interesting relationship between the

initial nutation and the oscillatory frequency of θ where at a high initial nutation, an inverse relationship is observed however at a low initial nutation they appear to have a direct relationship. This is likely due to the fact that at a high θ_0, the large precession rate will result in more rapid, stable motion of the disk however at a low θ_0, the disk is less stable in its precession and its nutation tends to vary more dramatically but at a slower rate. Figure 4.10 and Figure 4.13 indicate that the same applies to the xy-plane drag where higher drag coefficients lead to a lower frequency of oscillation of θ. The same does not appear to apply to changes in C_z, in fact the opposite appears to be the case. A higher drag in the z-direction appears to lead to a larger oscillatory frequency. All forms of drag coefficient in all directions, however, expectedly lead to very fast damping of the amplitude of oscillation of θ.

5.4. The approximated frictional model

The model used to take friction into account was an approximate answer to the question of how damping effects the motion of the disk. In reality there is air drag, surface friction between the disk and the surface, and potentially many other damping forces in effect. The surface friction is assumed to be zero (due to no slip) and the sum of all of the other damping forces are approximated as a drag induced torque (as in Equation 1.8) which is proportional to the inertia tensor of the disk and the square of the disk's angular velocity and is moderated by drag coefficients. This is a simplistic model which obviously neglects the finer details of the material used, and the precise relationships involved as well as the calculations of the actual drag coefficients due to the sheer complexity involved being beyond the scope of this project (likely involving analysis of material properties and fluid dynamics to analyse the air drag).

5.5. The error prone Lyapunov exponent

The Lyapunov exponent is a concept that applies primarily to exponential systems due to its characteristic equation deriving from an assumption of exponential growth. This inherently applies less accurately to systems which do not fit well to an exponential. This appears to be the case for the spinning disk system as the graphs in Figure 4.7 should ideally be close to perfectly linear but with varying slopes (if the distance between paths truly diverged exponentially). Looking at these figures and taking the regular oscillations as outliers, it can be seen that the increase is very roughly linear. The pattern however deviates frequently from this line making it very difficult to simply discount these frequent oscillations as just outliers, particularly when it comes to data analysis. This means that, as described above, the particular range of datapoints which one approximates to a line and uses to calculate λ is extremely subjective and error prone. The best analysis one can hope to achieve using Lyapunov exponents in the case of the spinning disk system involves looking at the graphs, selecting the best range available to approximate to a line based on reasonable criteria, and using those same criteria to select the range for all values of θ_0. This does not solve the issue of the specific λ values being highly subjective and error prone, however, it does achieve a level of internal consistency between the values found for λ which is useful in modelling how the relative chaos of the spinning disk system changes with initial nutation. In order to more effectively measure the degree of chaos of the system, it is recommended that the Lyapunov method is somehow refined to better suit the spinning disk system or potentially for a different method other than Lyapunov exponents to be used.

5.6. Chaotic nature of the system relative to the initial nutation

From Figure 4.14 looking at the bigger picture (5.14a), it is easy to see that the relative sensitivity of the system to the initial conditions is roughly the same for most values of θ_0 until close to 90° at which point any very small changes in the initial nutation very significantly affect the system dramatically.

However, looking more closely at the behaviour throughout the full range of θ_0 values (5.14b), it is clear that there is notable variation in the relative sensitivity, with local minima/maxima at the angles of 30°, 45° and 66°. It is tempting to look at the geometric significance of 60° angles fitting in more succinctly with 30° and 45°. The graph displays an interestingly sinusoidal behaviour, peaking at the exact centre of the range of possible θ_0 values.

It is worth pointing out the omission of $\theta_0 < 28°$ values. The reason for this was due to an inherent instability in the code which assumed one contact point between the surface and the disk. When the initial nutation is low enough combined with a low precession rate, the disk falls flat before it is able to enter a stable precession motion and thus the contact point is undefined as all points on the surface of the disk are contacting the opposing surface. This naturally leads to an indexing error in MATLAB. The exact nutation threshold below which the code cannot handle depends on the rate of precession. Intuitively if the disk is spun at a high enough rate even at a very low initial nutation, the disk will be able to reorient itself at a high angle of nutation (as described in section 6.3) before it falls flat thus allowing it to continue spinning. The necessary rate of precession to accomplish lower and lower initial nutations, however, quickly becomes unrealistically large and this generates its own problems. The best compromise found was to set the precession rate to

$80\ revolutions\ t^{-1}$ allowing nutations just lower than 30° to illustrate the symmetry of the behaviour about the 45° line without having an overly large precession rate.

5.7. Why do these local extremes appear?

Looking at the graphs from Figure 4.15 to Figure 4.17, it could be ascertained that the retrograde pattern referenced by Jalali et al. [1] is related to the local extremes of sensitivity to initial perturbations. As the angle approaches $\theta = 30°$ and $\theta = 66°$ the retrograde appears to become more pronounced (with the motion entering retrograde earlier along the trajectory) whereas around $\theta \approx 45°$ the retrograde is less pronounced (with the trajectory appearing to "unravel" as θ is increased). It could potentially be that a low level of retrograde / a later retrograde may be somehow associated with high sensitivity of the system to changes in the initial conditions

An important point to note is the inconsistency of the time range used to produce the trajectory in 5.15a ($t = 0\ to\ t = 6.99$) as opposed to the time range used to produce every other graph ($t = 0\ to\ t = 50$). The reason for this exception relates to the error described in Section 6.6; the simulation failed after $t = 7$ with an indexing error, implying that the disk had fallen flat after that time period. The reason why this became an issue now but not when measuring the Lyapunov exponent is that for the previous measurement, the time range of $t = 0\ to\ t = 0.05$ was used to calculate the initial behaviour of $\ln(d_t)$ vs t. This made it appear as if the disk had settled into a stable motion but in reality, it simply took longer than $0.05t$ for the disk to fall flat. It could be that there is some proneness for the disk to fall flat up until the $\theta = 45°$ mark at which point the disk is upright enough that it is more likely to continue spinning indefinitely due to the lack of surface friction. The other extreme would involve the disk being highly likely to fall flat ($\theta = 30°$) or highly likely

to continue spinning in a stable motion ($\theta = 66°$). This minimum is observed on the graph at $\theta = 66°$, however, it is also possible that this section of the graph (on either side of $45°$) is symmetric and the "virtual minimum" is closer to $60°$. This difference between this virtual minimum could be explained by observing the apparent tendency of the sensitivity to increase dramatically close to $\theta = 90°$. This tendency presumably has a negligible effect at low values of θ but the extent to which this tendency influences the behaviour of the overall sensitivity may increase slowly as θ increases until it becomes less and less negligible. As this influence grows to be on the order of the influence of the uncertainty relating to whether the disk stabilises or falls flat, the overall sensitivity shown in Figure 4.14 may increase slightly. This may explain the asymmetry in the behaviour of the sensitivity about $45°$ as the virtual minimum is being "pulled" towards the observed minimum by the increasing sensitivity near $90°$.

6. Conclusions

The spinning disk system is clearly one that is highly sensitive to the initial conditions of the Euler angles, their rates of change and the friction between the disk and the surface. The most affective of these variables are the initial nutation θ, the initial precession rate $\dot{\phi}$, the drag coefficients C_x, C_y, C_z and the initial revolution rate $\dot{\psi}$. The initial nutation appears to largely determine the overall amount of orbiting or rocking motion of the disk throughout its orbit as well as which one is more dominant. The tendency of the nutation of the disk to oscillate at a very high frequency is observed more at higher initial nutations.

The initial precession rate is the largest determining factor when it comes to the overall distance travelled by the disk throughout its motion. A high precession rate also increases the oscillatory frequency of θ, so that $\dot{\phi} \propto \nu_\theta$ however this relationship is only observed

at higher values of θ_0; at lower values this relationship is inverted so that $\dot{\phi} \propto \frac{1}{\nu_\theta}$. Further analysis is needed to determine the precise relationship (e.g. inverse law, inverse square law, etc.).

The initial revolution rate dramatically increased the distance travelled by the centre of mass when it was the more dominant spin component acting on the disk, however, this effect could be cancelled out by increasing the precession rate to be of the same order. The system is also significantly more sensitive to changes in the precession rate when the revolution rate is also high.

Increasing the drag coefficients C_x and C_y led to significantly less initial orbiting of the centre of mass and also to a greater frequency of oscillation of θ $\left(C_x, C_y \propto \nu_\theta\right)$. The xy-plane drag also appears to contribute far more to the overall damping of the disk motion than C_z does. The effects of increasing C_z appear to almost directly mirror those of increasing C_x and C_y whereas high C_z leads to significantly more initial orbiting, a lower oscillatory frequency of θ $\left(C_z \propto \frac{1}{\nu_\theta}\right)$ and does not significantly impact the overall damping.

The relative sensitivity of the system to the initial nutation reaches local minima at angles of $\theta_0 = 30°, 66°$ and reaches a local maximum at $\theta_0 = 45°$; exactly halfway into the total range of θ. This appears to be related to the level of retrograde experienced by the centre of mass motion where a low/late retrograde effect is associated with high sensitivity to initial nutation. The sensitivity then appears to increase dramatically as the initial angle approaches $\theta = 90°$. It is possible that this increase has the effect of dragging the apparent minimum from its true location to the observed location of $66°$

7. Appendix

θ	λ	θ	λ	θ	λ
28	72.6450	**49**	136.7544	**70**	81.5838
29	70.6024	**50**	126.0812	**71**	83.7317
30	68.5794	**51**	122.2405	**72**	86.7674
31	72.0817	**52**	120.3661	**73**	88.5410
32	77.2120	**53**	113.6397	**74**	95.8728
33	85.5336	**54**	109.9399	**75**	99.0506
34	91.7740	**55**	107.6846	**76**	107.5283
35	98.0402	**56**	104.8207	**77**	109.9647
36	105.2798	**57**	97.6202	**78**	113.7994
37	107.0649	**58**	94.6429	**79**	127.4730
38	112.8604	**59**	93.2903	**80**	147.8338
39	122.9429	**60**	92.2087	**81**	164.9343
40	129.5178	**61**	89.2437	**82**	186.3686
41	136.8976	**62**	85.3296	**83**	205.6586
42	148.8340	**63**	81.9046	**84**	271.4705
43	152.5570	**64**	81.5086	**85**	275.8553
44	167.0119	**65**	78.3085	**86**	379.4066
45	173.2172	**66**	77.7820	**87**	631.5421
46	163.9791	**67**	77.8301	**88**	890.1528
47	153.0496	**68**	78.7930	**89**	2.3242e+03
48	143.2071	**69**	79.6218		

Table 7.1: Recorded Lyapunov exponent for spinning disk system vs initial nutation

$\boldsymbol{\theta}$	$\boldsymbol{\lambda_{rel}}$	$\boldsymbol{\theta}$	$\boldsymbol{\lambda_{rel}}$	$\boldsymbol{\theta}$	$\boldsymbol{\lambda_{rel}}$
28	1.059283	**49**	1.994103	**70**	1.189625
29	1.029499	**50**	1.83847	**71**	1.220945
30	1	**51**	1.782467	**72**	1.265211
31	1.051069	**52**	1.755135	**73**	1.291073
32	1.125877	**53**	1.657053	**74**	1.397982
33	1.24722	**54**	1.603104	**75**	1.44432
34	1.338215	**55**	1.570218	**76**	1.567939
35	1.429587	**56**	1.528458	**77**	1.603465
36	1.535152	**57**	1.423462	**78**	1.659382
37	1.561182	**58**	1.380049	**79**	1.858765
38	1.64569	**59**	1.360325	**80**	2.155659
39	1.792709	**60**	1.344554	**81**	2.405012
40	1.888582	**61**	1.301319	**82**	2.71756
41	1.996191	**62**	1.244245	**83**	2.998839
42	2.170244	**63**	1.194303	**84**	3.958485
43	2.224531	**64**	1.188529	**85**	4.022422
44	2.435307	**65**	1.141866	**86**	5.53237
45	2.525791	**66**	1.134189	**87**	9.208918
46	2.391084	**67**	1.13489	**88**	12.97989
47	2.231714	**68**	1.148931	**89**	33.89064
48	2.088194	**69**	1.161016		

Table 7.2: Normalised Lyapunov exponent for spinning disk system vs initial nutation

8. Contribution Checklist

	Myself	Others	Comments
Research and Literature Review			
Review of research papers on the topic	80%	20%	Supervisor provided copies of two research papers on the dynamics of rolling rings.
Research into mechanics of rigid bodies	90%	10%	Supervisor recommended *Classical Dynamics of Particles and Systems, Chapter 11*.
Code Design and Preparation			
EqOfMotionModel.m	10%	90%	Supervisor wrote the model to simulate the motion and I adjusted the code to model λ
LyapunovExponentPlotter.m	100%	0%	I wrote a separate code file to record and plot λ
Debugging			
Debugging EqOfMotionModel.m	50%	50%	I debugged some initial issues relating to the variation of the initial position of the COM due to changes to θ_0
Inability to lower θ_0 past a certain threshold	50%	50%	My supervisor clarified that this issue was due to an inherent instability with the models determination of the contact point in the code.
Analysis			
System sensitivity analysis	100%	0%	I generated graphs to visualise the system behaviour and analysed the chaotic nature of the system.
Discussion			

Discussion of results and conclusions	100%	0%	I qualitatively described the significance of the graphs generated and the potential errors involved.

9. References

[1] Jalali, M.A., Sarebangholi, M.S., Alam, M.-R. (2019) Terminal Retrograde Turn of Rolling Rings [online], Physical Review, available: https://journals.aps.org/pre/abstract/10.1103/PhysRevE.92.032913 [accessed 13 Oct 2019].

[2] Leine, R.I. (2009) 'Experimental and theoretical investigation of the energy dissipation of a rolling disk during its final stage of motion', Archive of Applied Mechanics, 79(11), 1063–1082.

[3] Ma, D., Liu, C., Zhao, Z., Zhang, H. (2014) 'Rolling friction and energy dissipation in a spinning disc', Proceedings of the Royal Society A: Mathematical, Physical and Engineering Sciences, 470(2169), 20140191.

[4] Press, W.H., Tevkolsky, S.A., Vetterling, W.T., Flannery, B.P. (2007) Numerical Recipes: The Art of Scientific Computing, 3rd ed, Cambridge University Press.

[5] Thornton, S.T., Marion, J.B. (2004) Classical Dynamics of Particles and Systems, 5th ed, Cengage.

[6] Walsh, P., Clancy, I. (2020) The Dynamics of Spinning Disks on Frictional Surfaces [online], University Of Limerick, available: https://github.com/PatrickWalsh90598/The-dynamics-of-spinning-disks-on-frictional-surfaces.